Bedload transport in bedrock rivers: the role of sediment cover in grain entrainment, translation and deposition

Rebecca A Hodge [ab*], Trevor B Hoey [a] and Leonard S Sklar [c]

[a] School of Geographical and Earth Sciences, University of Glasgow, University Avenue, Glasgow, G12 8QQ, UK

[b] Department of Geography, Durham University, Science Laboratories, South Road, Durham, DH1 3LE, UK

[c] Department of Geosciences, 622 Thorton Hall, San Francisco State University, 1600 Holloway Avenue, San Francisco, California 94132, USA

[*] Corresponding author
Email: rebecca.hodge@durham.ac.uk
Telephone: +44 (0) 191 334 1800
Fax: +44 (0) 191 334 1801

Revised manuscript for Journal of Geophysical Research – Earth Surface. Final version 28 September 2011.

12 figures; 1 table.

Keywords: Bedrock river, sediment transport, sediment cover

Abstract (up to 250 words)
Bedrock rivers exert a critical control over landscape evolution, yet little is known about the sediment transport processes that affect their incision. We present theoretical analyses and field data that demonstrate how grain entrainment, translation and deposition are affected by the degree of sediment cover in a bedrock channel. Theoretical considerations of grain entrainment mechanics and sediment continuity each demonstrate that areas of exposed bedrock and thin sediment depths cause sediment transport to be size-independent, albeit excluding extreme grain sizes. We report gravel and cobble magnetic tracer data from three rivers with contrasting sediment cover: the bedrock River Calder (20 % cover), the bedrock South Fork Eel River (80 %) and the alluvial Allt Dubhaig (100 %). These datasets show that: 1) transport distances in the River Calder are controlled by sediment patch location, whereas in the other rivers transport distances are described by gamma distributions representing local dispersion; 2) River Calder transport distances are size-independent across all recorded shear stresses, whereas the other rivers display size-selectivity; 3) River Calder tracers are entrained at a dimensionless shear stress of 0.038, which is relatively low compared to alluvial rivers; and, 4) virtual grain velocities in the River Calder are higher than in a comparable reach of the Allt Dubhaig. These contrasts result from differences in the thicknesses and spatial distribution of sediment in the three rivers, and support the theoretical analysis. Sediment processes in bedrock rivers systematically vary along a continuum between bedrock and alluvial end members.

1 Introduction

Incision of bedrock rivers is a key process driving landscape development through setting the local base-level [*Whipple*, 2004; *Stark et al.*, 2009]. A major control on bedrock erosion is the interplay between sediment cover and erosive mobile grains [*Sklar and Dietrich*, 2004; *Finnegan et al.*, 2007; *Johnson and Whipple*, 2007; *Turowski et al.*, 2007]. This interplay depends on processes operating over a range of scales, from single-event erosion and deposition through to long-term changes in sediment supply regimes and consequent morphological adjustment of the channel [*Gasparini et al.*, 2004; *Lague*, 2010]. Process-based models of saltation-driven incision focus on the short-term dynamics of individual grains [*Sklar and Dietrich*, 2004, 2006; *Turowski et al.*, 2007; *Turowski*, 2009]. A bedrock river is rarely entirely free from sediment cover; we use the term bedrock river to encompass the range of mixed alluvial-bedrock channel bed conditions [*Turowski et al.*, 2008]. Consequently, mobile grains in a bedrock channel will typically be transported across both alluvial and bedrock surfaces. The extent of sediment cover is a result of the sediment flux supplied to the channel and the channel transport capacity, although the form of this relationship is debated [*c.f. Sklar and Dietrich*, 2004; *Johnson and Whipple*, 2007; *Turowski et al.*, 2007; *Cowie et al.*, 2008]. Furthermore, the pattern of sediment cover can respond dynamically in response to both flow and sediment flux fluctuations [*Chatanantavet and Parker*, 2008; *Johnson et al.*, 2009; *Lague*, 2010].

During a single transport event, comprising grain entrainment, translation and deposition, a grain may interact with both bedrock and alluvial surfaces. The relative proportion of these surfaces depends on the quantity of sediment in the channel and on channel morphology; sediment cover can vary between zero and complete cover, as in Figure 1 [*Howard and Kerby*, 1983; *Montgomery et al.*, 1996]. As sediment cover develops on a rock surface, dispersed patches and bars, which are typically one or two grains thick, form first. As sediment volume increases, sediment patches grow in both areal extent and depth [*Chatanantavet and Parker*, 2008], leading to bars forming that can be a metre or more thick [*Tinkler and Wohl*, 1998; *Jansen*, 2006]. With low sediment volumes, there is little reach-scale variation in grain size distribution whereas with higher volumes sediment thickness becomes sufficient for armouring and vertical size segregation to develop [e.g. *Goode and Wohl*, 2010a].

Sediment transport is influenced by, amongst others, surface roughness and grain sheltering effects, the possibility for grain burial and the velocity profile of the overlying flow. Alluvial channel surface roughness is a function of the surface grain size distribution and, via grain sheltering effects, affects the relationship between grain size and critical entrainment shear stress [*Kirchner et al.*, 1990; *Buffington et al.*, 1992; *Frey and Church*, 2010]. Surface roughness also affects the probability of grain deposition, and hence the distance of grain translation [*Einstein*, 1950; *Habersack*, 2001; *Wong et al.*, 2007]. The thick active layer (i.e. sediment that participates in bedload transport) in an alluvial channel enables grains to be deposited at depth in the bed, which can be a size-selective process and inhibits subsequent entrainment [*Ferguson and Hoey*, 2002; *Pyrce and Ashmore*, 2003a]. Surface roughness also affects the flow velocity profile and so influences entrainment via the force exerted on a grain [*Grass*, 1970; *Papanicolaou et al.*, 2001; *Schmeeckle and Nelson*, 2003].

In bedrock channels, the mosaic of bedrock and sediment cover means that the properties listed above can show large spatial variation. For example, the morphology of bedrock surfaces ranges from flat to complex 3D forms [*Wohl and Ikeda*, 1997; *Whipple*, 2004]. Complex topography can affect the local flow structure [*Finnegan et al.*, 2007; *Johnson and Whipple*, 2007]. Areas of the channel without sediment or with thin sediment layers exclude the potential for grain burial. Laboratory data show that grain velocities and step length are greater over non-erodible beds than over mobile beds [*Lajeunesse et al.*, 2010]. There are therefore several reasons to expect that the components of sediment transport will operate differently in alluvial and bedrock areas of the channel. Further, the proportion and distribution of alluvial and bedrock surfaces in a bedrock river will significantly affect the rate and grain-size specificity of sediment transport processes within that channel.

To date, there are limited field data with which to constrain sediment transport processes in bedrock channels. *Goode and Wohl* [2010b] found that transport distances of sediment tracers were size dependent transport in a reach with bedrock ribs longitudinal to flow, but size-independent when the ribs were oblique to flow. The former result is consistent with much alluvial river data [e.g. *Hassan et al.*, 1991; *Wilcock* 1997; *Ferguson et al*. 2002; *Pyrce and Ashmore* 2003b], whereas the latter demonstrates the influence of the bedrock ribs on grain transport processes. *Siddiqui and Robert* [2010] also reported size-dependent transport lengths in a bedrock reach with high alluvial cover.

The position of a channel along the continuum between zero and complete sediment cover is a key variable in bedrock incision models [*Sklar and Dietrich*, 2004, 2006; *Turowski et al.*, 2007]. Consequently, there is a need to both theorise and quantify how the spatial extent of sediment cover in bedrock rivers affects sediment transport processes. We approach this task firstly by considering how the presence of a bedrock surface will affect the components of sediment transport. We do this both using *Kirchner et al.*'s [1990] model of grain entrainment and through analysis of sediment continuity. These theoretical considerations are then used to interpret sediment tracer data from three rivers with different sediment cover: the River Calder (20 % sediment cover), the South Fork Eel River (80 % sediment cover) and the Allt Dubhaig (100 % sediment cover) [*Ferguson et al.*, 2002]. Finally, we discuss the implications of the theoretical and field results for modelling bedrock incision.

2 Theoretical Framework

2.1 Sediment cover continuum

The development of, and dynamic change in, sediment cover in a bedrock channel are driven by grain entrainment (E), translation (T) and deposition (D). These processes vary depending on whether a grain is on a bedrock or alluvial surface (e.g. entrainment from an alluvial surface, E_a, or a bedrock surface, E_b). A single grain movement, comprising entrainment, translation via saltation, and deposition, can therefore be described by one of eight possible combinations. The combination of $E - T - D$ that a grain experiences depends on the extent of sediment cover in the channel, ranging from $E_a - T_a - D_a$ at the fully alluvial end member to $E_b - T_b - D_b$ in the pure bedrock case (Figure 1). Given the proposed distributions of sediment cover, three of the eight combinations are unlikely to occur. To understand how the extent of sediment cover affects both the total flux and its grain size distribution in rivers across

the spectrum in Figure 1, we extend established theory to predict how each of entrainment, translation, deposition and net mass continuity will vary between the bedrock and fully alluvial cases.

2.2 Grain entrainment

Except in the rare case of extremely low sediment cover, sediment forms patches on the bed of a bedrock river rather then being multiple isolated grains. Such grouping occurs because grains accumulate in areas of the channel where the bed roughness, hydraulics and the sheltering influence of other grains increase grain stability [*Finnegan et al.*, 2007; *Johnson and Whipple*, 2007; *Chatanantavet and Parker*, 2008]. Consequently, initial grain entrainment primarily occurs from alluvial surfaces, i.e. E_a is far more probable than E_b, regardless of the extent of sediment cover. During a transporting event, a mobile grain may undertake multiple steps before being deposited in a stable position [*Einstein* 1950; *Drake et al.*, 1988], where each step itself contains multiple saltation hops [*Sklar and Dietrich*, 2001; *Attal and Lavé*, 2009]. In a river with low alluvial cover, the initial step for a grain in an event is most likely to involve entrainment from an alluvial surface, but subsequent (and hence the majority of) entrainments are more likely to be from bedrock surfaces.

Differences between E_a and E_b reflect the effect of the underlying surface geometry on the grain position and hence critical entrainment shear stress (τ_c). We quantify this effect on τ_c by using a Monte Carlo application of the model of *Kirchner et al.* [1990], which calculates τ_c for a grain by solving the force balance at the threshold of motion:

$$\frac{F_D}{\tan\Phi} + F_L = F_W = \frac{1}{6}\left(\rho_s - \rho\right) g \pi d^3 \qquad (1).$$

F_D and F_L are respectively drag and lift forces, F_W is the immersed weight of the grain, Φ is the grain pivoting angle which describes pocket geometry, ρ_s is the density of sediment (taken as 2650 kg m^{-3}), ρ is the density of water, g is acceleration due to gravity and d is the grain diameter. F_D and F_L are calculated assuming a logarithmic flow velocity profile and incorporate both grain exposure and elevation with respect to the local velocity profile. The boundary shear stress at the threshold of motion, τ_c, is calculated by expressing F_D and F_L in terms of τ_c, and substituting into and rearranging equation (1); for the full derivation see *Kirchner et al.* [1990].

In *Kirchner et al.*'s [1990] model, the underlying surface is assumed to be a granular material with grain size K (Figure 2), and its effect on τ_c is expressed through the values of Φ, F_D and F_L. By applying idealised geometrical relationships [*Kirchner et al.*, 1990] and relationships derived from field data [*Johnston et al.*, 1998], Φ, F_D and F_L can be expressed as functions of the relative sizes of the overlying grain (d) and the representative grain size of the underlying surface (K). When a grain is entrained from an alluvial surface (E_a), both d and K are drawn from the same grain size distribution (GSD) (Figure 2a). For illustration we use a measured lognormal sediment GSD from the River Calder (mean 5.56 ψ; standard deviation 0.69 ψ, where $\psi = \log_2(d)$ and d is measured in mm).

For entrainment from a bedrock surface (E_b), the local roughness of the bedrock surface is represented as an appropriate value of K. Bedrock surface roughness is very variable, from relatively smooth abraded surfaces to irregular plucked and jointed surfaces [e.g. *Goode and Wohl*, 2010b]. However, at the scale of an individual grain, most bedrock surfaces will be locally smooth so we omit the effect of macroscale

roughness on local velocity profiles and represent these as a surface composed of roughness elements that are finer than the GSD of the overlying grains (Figure 2). To estimate the representative GSD of the roughness elements, bedrock roughness was calculated from high-resolution topographic profiles ~ 3m long in total, measured in the River Calder. Roughness was quantified as the standard deviation of elevations (σ_z) within multiple 50 mm lengths of the profiles; 50 mm is the median alluvial grain size (d_{50}), and so roughness is measured at a scale relevant to individual grains. Each value of σ_z was converted to an equivalent grain size. All together, these equivalent grain sizes follow a lognormal GSD with a mean of 4.42 ψ and standard deviation of 0.99 ψ. Trends in the model results are not sensitive to the particular values of these parameters.

Our Monte Carlo application of *Kirchner et al.*'s [1990] model predicts τ_c for 1000 grains entrained from each of the alluvial (Figure 2a) and bedrock (Figure 2b) surfaces. In each case, 1000 pairs of an overlying and an underlying grain size are drawn at random from the respective distributions. d/K is used to calculate grain pivoting angle (Φ), exposure (e) and projection (p) [see Figure 2c and *Kirchner et al.*, 1990]. τ_c and dimensionless τ_c (τ_c*) are subsequently calculated for each grain, and the results are shown in Figure 3.

τ_c for grains on a bedrock surface is about an order of magnitude lower than for the same size grains on an alluvial surface (Figure 3); when $d = d_{50}$ and $K = K_{50}$, τ_c = 2.5 and 21.9 Pa for the bedrock and alluvial cases, respectively. *Dancey et al.* [2002] also observed an order of magnitude increase in τ_c* when grain packing density increased from 3 to 91 %, which is comparable to the difference between a bedrock and an alluvial surface. Re-entrainment during movement, E_b, therefore requires a significantly lower shear stress than the initial entrainment E_a. Consequently, for the same shear stress, excess shear stress (τ - τ_c) is greater for a grain in transport across a bedrock surface than for a grain on an alluvial surface.

Entrainment from a bedrock surface shows a weak dependence of τ_c on grain size; fixing K at K_{50}, τ_c decreases from 3.5 Pa for $d = d_{05}$ to 2.1 Pa for $d = d_{95}$. Model results are parallel tova line fitted by *Johnston et al.* [1998] to both theoretical and field data (Figure 3b). Along this line, τ_c* is proportional to 1/d, i.e. grains are equally mobile. The small dependence of τ_c on d is because changes in grain geometry as grain size increases mean that grains have lower pivoting angles, larger exposure and protrude higher into faster flow. Entrainment from a bedrock surface will therefore not be a major cause of size-selective transport. However, as entrainment is only one component of grain movement, other aspects may produce or inhibit size-selectivity.

In a bedrock river, E_a may be affected by the shallow sediment depths associated with low sediment cover. In an alluvial channel, surface coarsening acts to equalise τ_c for different grain sizes because smaller grains having relatively less exposure and higher pivoting angles than larger grains [*Wiberg and Smith*, 1987; *Kirchner et al.*, 1990; *Parker and Sutherland* 1990]. Thin sediment layers cannot develop surface coarsening thus reducing or eliminating this equalising effect, such that entrainment shear stress is primarily a function of grain size. Consequently, the exact functioning of E_a in a bedrock river may vary according to sediment depth.

Bedrock channels have slopes up to ten times greater than alluvial channels for a given drainage basin area [*Howard and Kerby,* 1983; *Montgomery et al.*, 1996]. Critical entrainment shear stress is usually assumed to be independent of channel slope. However, *Shvidchenko et al*. [2001], *Lamb et al.* [2008] and *Recking* [2009] have demonstrated a significant effect of slope with the same size of grain being more stable on a steeper slope. This effect is due to slope dependence of the velocity profiles for a given discharge, and to the changes in the grain force balance due to relative roughness and partial grain emergence. Thus, the typically steeper nature of bedrock channels implies that grain mobility from alluvial patches in bedrock rivers will be reduced compared to alluvial cases.

2.3 Grain translation

As excess shear stress (τ - τ_c) is higher over bedrock surfaces than alluvial ones grain dynamics differ over the two surfaces (T_a and T_b). For example, saltation height, length and downstream velocity are each functions of $\left(\tau^* - \tau_c^* / \tau_c^*\right)^a$, where $a < 1$ [*Sklar and Dietrich*, 2004]. *Lajeunesse et al.* [2010] showed that grain velocities and step lengths are larger over non-erodable (i.e. bedrock) surfaces than over mobile alluvial surfaces. The properties of a bedrock surface also affect saltation dynamics as there will be few, if any, particles to be entrained by an impacting grain. Further, grain rebound is affected by the coefficient of restitution and the distribution of angles of the bedrock surface impacted by mobile grains. Hence, grains moving over a bedrock surface will undergo longer, more frequent, translation steps than grains on an otherwise equivalent alluvial bed. Consequently, for the same shear stress, sediment transport capacity will be higher over bedrock surfaces.

2.4 Grain deposition

Grains are more likely to be deposited on an alluvial surface (D_a) than on a bedrock surface (D_b); the higher grain pivoting angles and lower exposures predicted by the *Kirchner et al.* [1990] model for the alluvial surface enhance deposition as well as impeding entrainment. In addition, grain roughness could also affect the local flow profile, decreasing shear stress and enhancing deposition. Consequently, in a bedrock channel with low sediment cover, deposition is mainly determined by sediment patch location. Deposition on a bedrock surface may occur as flow recedes, when translation is halted as shear stress falls before grains have reached an alluvial area.

Sediment patch location is controlled by the interaction between local channel morphology and flow hydraulics. For example, patches may develop where the macroscale topography reduces local flow velocities, such as between bedrock ribs and within potholes [*Goode and Wohl*, 2010a; 2010b]. Sediment patches are therefore unlikely to exhibit the regular spacing of alluvial bedforms and bars. Once areas of sediment are established, the decreased probability of re-entrainment of grains from these areas provides positive feedback promoting their maintenance [*Johnson and Whipple*, 2007; *Finnegan et al.*, 2007].

Under low sediment cover, grains will mainly travel between areas of sediment, and so grain transport lengths will be determined by the inter-patch spacing. As sediment cover increases, the probability of deposition becomes more spatially uniform and the location of deposition is increasingly driven by processes identified in alluvial rivers [*Pyrce and Ashmore,* 2003b; *Hassan et al.,* 1991]. The greater depth of sediment in

alluvial rivers, and in bedrock rivers with higher sediment cover, also increases the potential for grains to be deposited at depth within the bed, thus reducing their probability of subsequent entrainment [*Ferguson and Hoey*, 2002].

2.5 Sediment continuity

All components of $E - T - D$ show important differences between bedrock and alluvial surfaces, which will affect event-scale sediment movement. We now assess how these differences affect the long-term relative behaviour of different size fractions and the long-term conditions under which a bedrock river could have steady state sediment cover. While our previous analysis treated sediment transport as a discrete process, we now turn to analysis of sediment continuity.

The presence (or absence) of size selectivity in sediment transport is important because it links the volumes and GSDs of the incoming sediment, the sediment on the channel bed and the sediment transported out of the channel, and can result in aggradation or degradation. Size selectivity can occur in different components of sediment transport, including grain entrainment, velocities, frequency of motion and deposition. Here we focus on grain size dependence in grain travel distances, which is consistent with our use of gravel tracers.

We extend the standard continuity (Exner) equation expressed for individual size fractions of bed sediment [*Parker* 1991] to the case of a bedrock channel with fraction of bedrock exposure F_e, sediment cover $1-F_e$ and uniform depth sediment deposits:

$$(1-\lambda)\left[\frac{\partial}{\partial t}\left(L_a F_i\right)\left(1-F_e\right)+\varepsilon_i \frac{\partial}{\partial t}(\eta - L_a)\left(1-F_e\right)\right] = -\frac{\partial}{\partial x}\left(q_{bT}\, p_i\right) \qquad (2)$$

λ is sediment porosity, L_a is the thickness of the active (surface) layer, η is bed surface elevation above bedrock, q_{bT} is the volumetric bedload transport rate per unit width (m^2s^{-1}). F_i, ε_i, and p_i are the fractional abundances of sediment in the i^{th} size class in the surface layer, the sediment that is exchanged between the surface and sub-surface layer during aggradation or degradation and the bedload, respectively. Equation (2) is consistent with that given by *Chatanantavet et al.* [2010], although it assumes that abrasion and lateral sediment inputs are zero. Changes in sediment storage in a bedrock channel can arise via changes in L_a, sediment GSD and F_e. If the mean sediment thickness ($z = <\eta>$) is greater than L_a, then a sub-surface layer and the potential for vertical variations in sediment GSD develop.

We initially consider the maintenance of steady state in a bedrock river with very thin alluvial deposits, so that z is less than the active layer thickness, L_a, and there is no sub-surface layer. Averaging over several flood events to eliminate the impacts of stochastic upstream sediment supply, the following simplifications apply:

$$\frac{\partial q_{bT}}{\partial x} \to 0 \qquad \frac{\partial\left(\eta - L_a\right)}{\partial t} \to 0 \qquad \frac{\partial\left(1-F_e\right)}{\partial t} \to 0 \qquad \frac{\partial L_a}{\partial t} \to 0 \qquad (3)$$

Under steady state, the first three conditions maintain the sediment volume in the reach. While an increase in η-L_a could be offset by a decrease in 1-F_e, this is unlikely because η-L_a and 1-F_e will normally be positively correlated. Furthermore, in any reach the bedrock morphology is likely to dictate an optimum storage configuration (i.e. values of 1-F_e and η-L_a) for a given sediment volume. The second condition also applies because there is no subsurface layer if $z < L_a$. The final condition is satisfied if

there is no change in the active layer GSD; L_a is generally assumed to scale with grain size, and in alluvial rivers is approximately $2d_{90}$ [e.g. *Parker* 1991; *DeVries*, 2002].

Under the limits from (3), (2) reduces trivially to

$$(1-\lambda)L_a\left[\frac{\partial F_i}{\partial t}\right] = -q_{bT}\frac{\partial p_i}{\partial x} \qquad (4).$$

Any change in the stored sediment grain size (F_i) thus is achieved by a spatial gradient in p_i, indicating the operation of size-selective entrainment and deposition. If a monotonic change in grain size persists for long time periods, F_i changes to produce coarsening (so reducing transport, inducing aggradation and development of full alluvial cover) or fining (increasing transport and transition to full bedrock exposure). To maintain steady state, both $\partial F_i/\partial t$ and $\partial p_i/\partial x$ must tend to zero.

The form of steady state in a bedrock river with $z < L_a$ will depend on the relationship between F_i and p_i. We envisage two possible forms. In the first, F_i is equal to p_i for all i, and so all grain sizes have the same probability of entrainment and deposition. This is broadly consistent with the *Kirchner et al.* [1990] model predictions of τ_c for grains on a bedrock surface. In the second form, the stored sediment in the reach is coarse relative to bedload entering the reach, however bedload entering and leaving the reach have the same GSD. The typical lower probability of entrainment for larger grains is offset by their higher abundance in the active layer and vice versa, producing no aggradation. For larger grains therefore $F_i > p_i$, with $F_i < p_i$ for smaller grains.

In alluvial rivers, a coarse surface layer enables grain-size dependent probabilities of entrainment to exist under steady state [*Parker and Sutherland*, 1990; *Allan and Frostick* 1999]. However, the development of such a layer requires $z > L_a$, which can only occur with relatively high sediment cover. Where sediment cover increases and F_e is low, a coarse surface layer may develop enabling grain-size dependent entrainment to operate in a bedrock river at steady state. If entrainment is correlated with grain size, over a given time period smaller grains will be entrained more frequently and will travel further than larger grains, subject to the relationship between grain size and translation distance.

We consider total travel distance, rather than solely entrainment, as our measurements are of total travel distances. We hypothesise that size-selectivity of travel distances in a bedrock river is caused by sorting taking place in alluvial areas of the bed, and thus that the degree of size selectivity is a function of the sediment storage volume in the reach, and hence of sediment cover $1\text{-}F_e$. This hypothesis is illustrated in Figure 4, which shows the possible range of size-selectivity of sediment transport distances from a minimum value of 0 to a theoretical maximum for a fully alluvial river. As $1\text{-}F_e$ increases, rivers are more likely to exhibit size-selectivity closer to the theoretical maximum, as shown by the increasing white area.

2.6 Use of tracers

Our theoretical analysis of the effect of sediment cover on transport dynamics in a bedrock river has considered both the short-term movement of individual grains and long-term, reach-averaged behaviour. Both analyses suggest that the volume of sediment in a bedrock reach, which is correlated with $(1\text{-}F_e)$ determines grain

dynamics and size-selectivity. Two new sets of tracer data from bedrock rivers are used here to evaluate the theoretical analyses.

Repeat mapping of magnetically tagged sediment grains quantifies sediment dynamics in alluvial rivers over the timescale of multiple events [*Hassan et al.*, 1984; *Ferguson et al.*, 2002]. Such data quantify locations and probability of entrainment and deposition, transport distances and the influence of grain size and flow magnitude; but within-event dynamics cannot be resolved. Tracer recovery rate affects data quality; in alluvial rivers recovery varies considerably due to the time intervals between searches and system scale. Low sediment volumes and low probabilities of deep tracer burial in small bedrock rivers facilitate tracer recovery [*Goode and Wohl*, 2010b].

It is easier to use field data to test predictions of grain-scale dynamics than to test the longer-term predictions from the continuity analysis. Collecting longer-term data is more problematic, with a higher probability of changing boundary conditions. But, focussing on short term data assumes that we do not need explicitly to consider stochastic forcing of discharge and sediment supply [e.g. *Lague*, 2010], and that extreme events, which are less likely in short term data, do not contribute significantly to the long-term dynamics.

3 Study sites and field methods

We present tracer data from three rivers of comparable size, slope and GSD along the bedrock-alluvial continuum (Table 1). All three rivers actively transport sediment, with regular flow events in the full mobility regime.

3.1 River Calder, Renfrewshire, Scotland (55° 49' N, 4° 41' W)

The bedrock River Calder drains a peat moorland catchment. The study reach, described in Table 1, has no lateral sediment supply. Downstream of this reach alluvial cover varies from 0 to 100 %, forming lateral bars and channel-wide patches (Figure 5). Bar location varies little between events, but their spatial extent changes. Measured sediment thickness ranges from one grain diameter up to ~2 d_{90} (Figure 5), although visual estimates of sediment depth in one deep pool were up to 0.5 m.

286 painted, numbered, magnetic tracers were created from River Calder gravel using 6 mm diameter neodymium magnets. The tracer sizes fall within five half psi size classes (b-axis (d) of 4.5 to 7 ψ, or 23 to 128 mm), which include 89 % of the surface GSD measured in a predominantly alluvial reach 1 km upstream. This alluvial source supplies sediment to the study reach. Nine percent of the GSD is finer than 23 mm, and hence unsuitable for the magnetic tracer technique. Tracers will move as bedload.

Throughout the 220 day study, flow depth was recorded at 10 minute intervals by two pressure transducers 46 m apart in the upper part of the reach. Bed shear stress (τ) was calculated assuming uniform flow as $\tau = \rho g R S$, where R and S are respectively hydraulic radius and water surface slope calculated from the pressure transducer data.

We installed tracers in the upstream end of the reach on three separate occasions: days 1 (16th February 2009), 88 and 110 of the study. The latter two installations were made to replenish tracers at the top of the study reach. The sequence of tracer emplacement and recovery and river shear stress (τ) are detailed in Figure 6. Of the 224 tracers emplaced on day 1, half of each size class were randomly placed as

isolated grains along a single transect across the full channel width at the top of the reach, and the other half were used to replace grains of comparable size and shape in existing gravel bars. 50 tracers were placed in the upstream transect on day 88, with 64 tracers places in gravel patches on day 110 (see Figure 6 for tracer GSD). Different installation positions show the effect of grain position on entrainment probability.

Tracer positions were remapped at low flow on ten occasions up to day 220 (Figure 6). Between searches there generally were up to two flow events above the threshold for movement of tracer-sized material (defined later); one period contained seven events, and the last contained seventeen. Prior to day 212, tracers were only found as far downstream as a pool 95 -120 m along the reach. In searches up to and including search 9 (day 155), we removed tracers found in this pool because our initial experimental aim was to investigate tracer movement only in the reach upstream of the pool. The large flow event between days 155 and 212 (Figure 6) transported tracers over 600 m through and downstream of this pool. Two searches (10a and 10b, days 212 and 220) were necessary to search this area adequately; search data from 10a and 10b are combined, and referred to as day 220.

We visually located most tracers, used a magnetometer to search for buried tracers and mapped them using differential GPS (dGPS). Transport distances were calculated between all consecutive known locations as the downstream distance along the channel centre-line, also mapped using dGPS. These distances are therefore the accumulation of an unknown number of individual steps. The tracer relocation error is up to 0.2 m due to both dGPS uncertainty and the location of the receiver relative to the grain; we use 0.2 m as the threshold for identification of tracer movement.

3.2 South Fork Eel River, California, USA (39° 43' N, 123° 39' W)

Our second site was the reach of the South Fork of the Eel River in the University of California Angelo Coast Range Reserve [*Seidl and Dietrich*, 1992; *Howard*, 1998; *Sklar and Dietrich*, 2004; 2006]. Through this 4 km section, the active channel is confined within a meandering bedrock canyon, flanked by flights of terraces that are spatially coincident with a series of knickpoints [*Seidl and Dietrich*, 1992; *Fuller et al.*, 2009]. The bed is predominantly covered by alluvial patches ranging in grain size from gravel to boulder; ~ 20 % of the bed area is broad bedrock exposures [see photograph in *Sklar and Dietrich*, 2004]. Through the study site, alluvial cover is typically complete immediately downstream of tributary junctions; further downstream of junctions bedrock exposure becomes more frequent and extensive. This pattern may reflect rapid breakdown of weak clasts supplied by tributaries. Study reach characteristics are in Table 1. The bedrock is dominantly mudstone with sandstone interbeds, and the coarse bedload material is primarily derived from upstream sandstone and conglomerate units.

We installed a total of 330 tracers at the upstream end of the study reach in 1996 and 1997. The painted, numbered, magnetic tracers were made by implanting 9 mm diameter, 10 mm thick, cylindrical ceramic magnets into quartzite clasts collected on the Yuba River. We used the durable quartzite because drilling to implant magnets often fractured the weak local rock. Half the tracers were installed in an alluvial section, and the other half were installed as small artificial patches placed on bare bedrock just downstream. Tracer grain sizes were matched to the surface GSD of a bar with d_{50} = 90 mm. We recovered tracers using a Schoenstedt magnetic locator

capable of detecting magnetic tracers up to c. 1 m burial depth. We searched for tracer grains during late summer low flow in 1997, 1998, and 1999 (Figure 7). Most recovered tracers were buried. We surveyed tracer recovery location to < 1m with a total station and reburied tracers to approximately the same depth. A hydrograph for the experimental period is in Figure 7.

3.3 Allt Dubhaig, Scotland (56° 51' N, 4° 14' W)

The Allt Dubhaig is a small fully alluvial stream (c. 2.5 km long study reach) that has a strongly concave long profile with net aggradation that drives rapid downstream fining [*Ferguson et al,* 1996; 2002]. *Ferguson et al.* [1996; 2002] emplaced a total of 1220 magnetically tagged tracer particles in six reaches along the study section, each of which had different median grain size and shear stress. The GSD of tracers in each reach was based on the local bed GSD ensuring that statistically significant numbers of tracers were present in each half-psi size class. Tracers were emplaced in 1991, mapped regularly for two years (1991-1993) and remapped in 1999 [*Ferguson et al,* 2002]. High recovery rates were achieved using magnetometers and mapping to < 1m precision used a network of monumented cross-sections and total station surveying. Of the six tracer sets used, set T3 [*Ferguson et al,* 2002; Table 1] has the most similar conditions to the River Calder in terms of d_{50} and bankfull reach Shields stress, and so is used for direct comparison here. See *Ferguson et al.* [2002] for further information.

4 Results

The tracer data are analysed to quantify the effects of sediment cover, grain size and flow magnitude on the components of sediment transport. As the data record the total sum of grain movement between tracer searches, most analysis considers the sum of entrainment, translation and deposition, although individual components are also addressed. The three datasets were obtained using differing experimental designs, but they are compared wherever possible.

4.1 Tracer entrainment

Frequent remapping of tracers in the River Calder (Figure 6) shows most events entrained <100% of tracers, enabling analysis of how tracer and flow properties affected initial entrainment. The longer time periods and large number of events between re-mappings in the South Fork Eel River and the Allt Dubhaig mean that the population of immobile tracers is far smaller and initial entrainment cannot be analysed.

In the River Calder, the probability of initial entrainment of a tracer depends on the tracer substrate (bedrock or alluvial), tracer size (d) and the maximum event shear stress (τ_{max}) (Figure 8a). For all tracers, logistic regression of whether or not a tracer was entrained (movement > 0.2 m) against d, τ_{max} and a binary of starting position (bedrock, 0, or alluvial, 1) gave p-values (coefficients, which indicate the direction of the relationship) for: d 0.052 (-0.007); τ_{max} < 0.001 (0.078); alluvial/bedrock < 0.001 (-1.022). The surface that a tracer starts on and shear stress are therefore significant at $\alpha = 0.05$, whereas grain size is not.

Although grain size is not significant in the entire dataset, probability of entrainment is proportional to grain size for tracers on alluvial surfaces, but not on bedrock surfaces. Logistic regression of entrainment against d just for grains starting on alluvial surfaces has p = 0.04; for just grains starting on bedrock, p = 0.81.

Tracers on, or buried in, an alluvial substrate are less likely to be entrained than those on a bedrock surface (Figure 8a). Entrainment rates from both surfaces increase with shear stress; at higher shear stresses (90 Pa) tracers on both surfaces have comparable probabilities of entrainment.

4.2 Tracer deposition

In the River Calder, tracer deposition demonstrates the same variation between bedrock and alluvial surfaces as entrainment. For all events, the probability of entrained tracers (transport distance > 0.2 m) being deposited on an alluvial surface is at least 0.78 (Figure 8b). Logistic regression of deposition on an alluvial surface against d and τ_{max} gave p-values (coefficients) for: d 0.971 (-0.0003); τ_{max} < 0.001 (0.034). This regression indicates that at higher values of τ_{max}, tracers are more likely to be deposited on an alluvial patch (seen in Figure 8b), and that tracer size does not influence deposition location.

4.3 Travel distances

4.3.1 River Calder

Although substrate affects the probability of initial entrainment, it does not affect subsequent travel distances. Paired comparisons (both parametric on log(L) and non-parametric on L) found for the majority of shear stresses no significant difference at experiment-wise confidence level p = 0.05 and comparison-wise confidence level p = 0.006. Non-significant differences were about 1 m, but the minimum detectable difference for 90 % reliability is ~ 4 m for these data. Where statistically significant differences were found (τ_{max} = 34.7 and 35.0 Pa), the differences were less than 2.5 m, and unlikely to influence broader patterns in transport length. For the subsequent analysis, data from tracers starting from different substrates are amalgamated.

We recorded 1416 individual transport distances. The number of individual transport distances measured for each tracer varies; of the 224 tracers installed on Day 1, all but two tracers were relocated at least once, with a median of seven and a maximum of ten times. Tracers were transported up to 650 m during the 220 day experimental period. The distribution of transport distance (L) for all 1416 measurements (i.e. all distances between consecutive relocations) is positively-skewed and approximately lognormal. Of these values of L, 52 % are under 0.2 m (the minimum distance necessary to identify transport), and a further 19 % under 2 m.

To assess L over longer time durations, while accounting for the large flow event in the final inter-search period and removal of tracers from the pool, we divided the tracer data into two sets. Set 1 contains the 222 tracers emplaced on day 1 and subsequently found up to Day 155 (i.e. including those that were removed from the pool). Set 2 contains the 74 tracers in the upstream end of the reach on Day 155 and thereafter found on Days 212 and 220.

Of the 222 tracers in Set 1, 8 % showed zero movement by day 155. A further 6 % were no longer in situ by Day 155 and are assumed to have been entrained but not subsequently relocated. The distribution of L is bimodal (Figure 9a), with the main mode at 0 to 10 m, and a secondary mode in a channel-wide pool at 90 to 110 m. The largest event (τ_{max} = 90 Pa) occurred on Day 180 and transported tracers from the top

of the reach downstream through the pool (Figure 5). This event is reflected in the distribution of L for 74 tracers in Set 2 (Figure 9b), which is more disperse than for Set 1, although still contains dominant modes interspersed with empty bins.

Gamma distributions have been fitted to alluvial sediment transport data and interpreted as representing local sediment dispersion [*Hassan et al.*, 1991; *Schmidt and Ergenzinger*, 1992]. To test whether River Calder data are described by local dispersion, we fitted gamma distributions to both Set 1 and Set 2 (Figure 9), using the Matlab function gamfit. Gamma distributions provide poor fits to the tracer data; the Kolmogorov-Smirnov test shows a significant difference between the data and gamma distribution with $p < 0.001$.

4.3.2 South Fork Eel River

Tracers in the South Fork River Eel were also installed on both alluvial and bedrock patches. However, there was no significant difference ($p = 0.14$) between distributions of log virtual velocity (see section 4.6) for tracers with the two contrasting starting conditions, and so the data are combined. We do, however, group tracer travel distances by year to account for annual variations in the hydrograph.

Tracers travelled furthest in 1996-1997, with comparable distributions of smaller distances in 1997-1998 and 1998-1999 (Figures 9c to e). ANOVA of $\log(L)$ (where $L > 0$) for all three years shows a significant difference ($p < 0.001$). Tukey-Kramer analysis reveals a significant difference between 1996-1997 and each of the latter two years, whereas the latter two years are not significantly different from each other. For 1996-1997 and 1998-1999, the Kolmogorov-Smirnov test indicates no significant difference between the field data and a gamma distribution fitted to the data ($p = 0.41$ and 0.66 respectively), whereas for 1997-1998, $p = 0.04$.

4.3.3 Allt Dubhaig

Figures 9f and g show distributions of L from reach T3 of the Allt Dubhaig over both two and eight years. Neither distribution of T3 travel distances is significantly different to a gamma distribution (two year data $p = 0.26$; eight year data $p = 0.63$).

4.4 Shear stress influence

4.4.1 River Calder

Tracers travelled further under the higher shear stresses experienced after Day 155 (Figure 9). Using all 1416 measurements, L increases as function of τ_{max}, which varies from 29 to 90 Pa; dimensionless shear stress, $\tau^* = 0.036$ to 0.111 (Figure 10). The relative effects of τ_{max} and duration of flow above threshold (d_t) cannot be separated because $\log(\tau_{max})$ and $\log(d_t)$ are highly correlated ($R^2 = 0.52$, $p = 0.017$).

Motion is initiated at a threshold shear stress (τ_c) of between 29 and 34 Pa. To estimate τ_c, we fitted a quadratic to describe τ_{max} as a function of $\langle L \rangle$ (Figure 10); this is comparable to fitting a threshold power function to $\langle L \rangle$ as a function of τ_{max}, but is better constrained. The quadratic tends to a minimum value of 30.7 Pa. We therefore determine τ_c to be 31 Pa with $\tau_c^* = 0.038$.

4.4.2 South Fork Eel River and Allt Dubhaig

In the South Fork Eel River, tracers travelled furthest in 1996-1997 (Figure 9c to e). Additional analysis indicated no appreciable difference in tracer movement between the first and second year after tracer installation; the increased travel distances in 1996-1997 are therefore attributed to the higher flows in this year (Figure 7). The large number of flow events between tracer mapping in South Fork Eel River means that it is difficult to quantify further the effect of shear stress on L, and that τ_c cannot be calculated from these data. In the Allt Dubhaig there were also multiple flow events between mappings. τ_c was estimated for the Allt Dubhaig by identifying a threshold flow that transported gravel > 16 mm (the size of the smallest tracer) into a bedload trap at the downstream end of the study reach.

4.5 Grain size influence

4.5.1 River Calder

The analysis of deposition demonstrated that, once entrained, tracers of all sizes are transported across bedrock and are unlikely to be deposited until they reach an alluvial patch. This interpretation is consistent with the lower shear stress necessary for grain entrainment on a locally smooth bedrock surface calculated using the *Kirchner et al.* [1990] model and suggests that contrasts in deposition probability are more important than transport velocity. If the probability of deposition is itself not size-dependent, L will therefore be independent of grain size.

The distributions of L for each of the five size classes are not significantly different (ANOVA of log(L) for the five size classes, where L > 0.2 m, gives p = 0.14). Regression analysis demonstrates that individual grain size is not significant; a regression of log(L) against log(d) (where L > 0.2 m) gives R^2 = <0.001 and p = 0.70. In both analyses, use of data only where L > 0.2 m excludes any effect of size-selectivity in initial entrainment.

d is also not important within events; for each measurement period the relationship between $\langle L \rangle$ and τ_{max} is independent of d (Figure 11; $\langle L \rangle$ is calculated from all values of L). Furthermore, results are reproduced between comparable events (e.g. three events at 35 Pa), suggesting generality of this trend. The distribution of log(L) for an event is also independent of grain size. ANOVA of the size-specific distributions of log(L) (where L > 0.2 m) for different τ_{max} shows no significant difference between size classes for all events; in each case, p > 0.006 where 0.006 is the comparison-wise p needed for experiment-wise confidence level p = 0.05.

4.5.2 South Fork Eel River

In contrast to the River Calder, the South Fork Eel River shows a decrease in annual $\langle L \rangle$ with increasing grain size (Figure 11). Due to the uneven number of tracers in different half-phi size classes, tracers are instead divided into four size class quartiles. ANOVA of annual log(L) for the four different size classes shows that in 1996-1997 and 1997-1998, the distributions of log(L) are significantly different between the size classes (respectively p = 0.042 and 0.007). For 1998-1999, p = 0.060, indicating borderline similarity between the size classes.

4.5.3 *Allt Dubhaig*

In the Allt Dubhaig over timescales of 2 and 8 years, mean travel distance decreased with increasing grain size across a range of excess shear stresses in each of six reaches [*Ferguson et al.*, 2002, Figure 11]. The rate of decrease consistently varies as a function of d/d_{50}, with a faster rate of decrease when $d/d_{50} > 1$.

4.6 Virtual velocities

4.6.1 *River Calder*

Tracer grains are stationary for large periods of time when flow is below threshold. Virtual velocities [*Hassan et al.,* 1992] can be used to account for the intermittency of above threshold flows, allowing for easier comparison between different rivers and hence rates of transport across different surfaces. For the River Calder data, virtual velocities (V) were calculated by dividing the total transport distances for all 222 tracers emplaced on Day 1 by the duration of competent flow ($\tau > \tau_c$) (Figure 12). Transport distances were calculated between the tracer emplacement on Day 1 and their last known position.

In the River Calder, τ_c (31 Pa) is exceeded 3.6 % of the time. The distributions of V for the data are similar across the five tracer size classes; ANOVA of distributions of V for the five size classes (where $V > 0$) gives p = 0.10. The relationship between d and V (where $V > 0$, d is in mm and V is in km yr^{-1}) is:

$$V = 8.09d^{0.05} \quad (5)$$

with R^2 of 0.0006 and respective 95 % confidence intervals for the coefficients of -1.4 to 17.6 and -0.23 to 0.34. It is noted that values of V are sensitive to the value of τ_c; for comparison, if τ_c = 32 Pa, mean V increases by 2.7 km yr^{-1} (31 %).

4.6.2 *South Fork Eel River*

Velocities were calculated for all tracers for the time between tracer installation and their last known position. In contrast to the River Calder, velocities show strong size dependence, larger grains travelling more slowly (Figure 12). The relationship is:

$$V = 1720d^{-2.03} \quad (6)$$

with R^2 = 0.17 and respective 95 % confidence intervals for the coefficients of -3460 to 6900 and -2.7 to -1.3.

4.6.3 *Allt Dubhaig*

Tracer velocities in the Allt Dubhaig are explained by a combination of τ^* and d/d_{50} [*Ferguson et al,* 2002]. They also recorded a significant slowdown in tracer velocities between the initial survey period (1991-3) and the longer period (1991-9) that is attributed to diffusion processes [*Ferguson and Hoey* 2002]. Allt Dubhaig data from 1991-3 fit the relationship:

$$V = 10.67d^{-0.23} \quad (7)$$

with R^2 = 0.02 and 95 % confidence intervals for the coefficients of -0.73 to 22.1 and -0.50 to 0.04 respectively.

Virtual velocities for the River Calder and Allt Dubhaig are compared using equations 5 and 7 to calculate V for the geometric mean of each of the five size classes present in both rivers. For the smallest size class (23 – 32 mm), V is 90% (4.5 km yr^{-1}) faster

693 in the River Calder than in the Allt Dubhaig. For the largest size class (91 – 128 mm)
694 V is 180% (6.6 km yr^{-1}) faster in the River Calder.

695 **5 Discussion**

696 Key differences have been identified between the River Calder, South Fork Eel River
697 and Allt Dubhaig datasets, particularly in terms of the frequency distributions of L and
698 the extent to which L is grain-size dependent. These contrasting behaviours reflect the
699 position of the rivers along the bedrock – alluvial continuum (Figure 1), and result
700 from the different ways in which E – T – D operate on alluvial and bedrock surfaces.

701 **5.1 Tracer transport distances**

702 Values of L integrate grain entrainment, translation and deposition. Distributions of L
703 can be described by gamma distributions in both the South Fork Eel River and reach
704 T3 of the Allt Dubhaig, but not in the River Calder. Data from all three rivers (Figure
705 9) show a comparable range of travel distances (apart from days 1 – 155 in the River
706 Calder), indicating that differences between the distributions are not because the River
707 Calder tracers have not travelled as far and/or not experienced such high flows.
708
709 In the River Calder, modal travel distances are comparable to the spacing of in-
710 channel sediment stores, reflecting the morphological control on translation and
711 deposition. Between days 1 – 155, L has two modal values; 0 – 10 m and 90 – 110 m.
712 The first mode is from relatively immobile tracers that were mainly found along the
713 channel edges, either on a bar or buried by gravel sheets. The second mode is from
714 deposition in the channel-wide, predominantly alluvial, pool at the end of the reach
715 (Figure 5). The irregular distribution of L between days 155 – 220 is also
716 morphologically controlled; tracers are primarily deposited in the alluvial patches
717 along the channel (Figures 5 and 8b). In summary, translation is mostly occurring as
718 T_b, and D_a is far more common that D_b.
719
720 The gamma distributions of L in the South Fork Eel River and Allt Dubhaig are
721 consistent with data from several alluvial rivers [e.g. *Hassan et al.*, 1991; *Schmidt and*
722 *Ergenzinger*, 1992], although other alluvial data have been approximated by different
723 statistical distributions [e.g. *Pyrce and Ashmore*, 2003a; *Bradley et al.*, 2010]. *Pyrce*
724 *and Ashmore* [2003a] suggest that the appropriate statistical distribution depends on
725 bed shear stress. However, the above distributions only reproduce the effect of local
726 sediment dispersion, and assume that the processes of entrainment, translation and
727 deposition operate in the same way across the channel, e.g. E_a, T_a and D_a occur
728 everywhere. Statistical distributions therefore do not account for morphological
729 effects [*Hassan et al.*, 1991; *Frey and Church* 2010]. Consequently, the River Calder
730 tracers are unlikely to approach a gamma distribution of travel distances over longer
731 time periods and greater dispersion.
732
733 In the River Calder, L is determined by the reach morphology affecting grain
734 translation and deposition; this morphological influence is not observed in reach T3 of
735 the Allt Dubhaig and is much weaker in the South Fork Eel River data which shows
736 some secondary modes that may be associated with bar locations (Figure 9). Although
737 the reach T3 data suggest that dispersion dominates over morphological effects, of the
738 ten Allt Dubhaig datasets (five reaches, with data from two and eight years in each)
739 [*Ferguson et al,* 2002], only four are not significantly different to a gamma
740 distribution ($p > 0.05$). Differences to a gamma distribution occur because channel

morphology controls L through deposition in bars and channel switching leading to some grains entering long-term storage [*Ferguson and Hoey*, 2002]. *Pyrce and Ashmore* [2003b] identified modes of L that were consistent with pool-bar spacing in several alluvial rivers, particularly at higher values of τ^*, suggesting a morphological control on travel distances and the potential for spatial variation in E_a, T_a and D_a. Morphological controls on grain transport processes are therefore important across the bedrock-alluvial spectrum, but there are likely to be significant differences in the factors influencing the morphology. In the River Calder and other bedrock rivers, the location of sediment stores is controlled by the interaction between the eroding river and reach geology [*Goode and Wohl*, 2010b]. In alluvial rivers, morphological controls are more likely to be autogenically produced.

5.2 Threshold shear stresses and virtual velocities

In the River Calder, initial grain entrainment occurred at $\tau_c = 31$ Pa ($\tau_c^* = 0.038$). This is within the range of values of τ_c^* measured in alluvial rivers, from c. 0.025 to > 0.07, and is consistent with initial entrainment primarily occurring from alluvial patches (i.e. E_a), although care needs to be exercised in comparing results generated using different methods [*Buffington and Montgomery* 1997]. The relatively low value of τ_c^* for the River Calder may reflect the sediment patches being more loosely packed than is usual for sediment in an alluvial channel; for loosely packed sediment, τ_c^* can be as low as 0.01 [*Fenton and Abbott*, 1977; *Dancey et al.*, 2002].

Theoretical analysis of grain entrainment (Figure 3) predicts that grains on a bedrock surface will be entrained at $\tau_c^* < 0.02$. Consequently, if the flow is sufficiently high to entrain grains from alluvial patches in a bedrock channel ($\tau_c^* > 0.038$), these grains are very likely to be re-entrained if they are transported onto a bedrock surface. The differing values of τ_c^* for alluvial and bedrock surfaces means that τ^*/τ_c^* will be higher over the bedrock surface, hence T_b will readily occur and D_b is very unlikely.

The difference in grain transport processes between bedrock and alluvial surfaces is reflected in the virtual velocities. Virtual velocities from the River Calder are significantly higher than those from a directly comparable reach of the Allt Dubhaig (Figure 12), suggesting different grain dynamics. The higher velocities in the River Calder could be because grains move for a greater proportion of the time when the flow is above threshold, or because they move further between initial entrainment and deposition. The low probability of D_b and ready occurrence of T_b in the River Calder are consistent with these explanations, but full understanding requires within-event transport path and velocity data from individual grains [e.g. *Lajeunesse et al.*, 2010].

5.3 Grain size effects

The extent to which the components of grain movement are size-selective will also affect the sediment dynamics. In the River Calder, E_a is weakly size selective. Initial entrainment is mainly as E_a because grains are preferentially deposited on sediment surfaces. The size-selectivity of E_a is consistent with much data from alluvial rivers [*Buffington and Montgomery*, 1997]. In contrast, entrainment from a bedrock surface (E_b) is not size-selective, which is consistent with results from the *Kirchner et al.* [1990] model (Figure 3). The longer time scales of the Allt Dubhaig and South Fork Eel River data prohibit explicit analysis of initial entrainment.

Distributions of L reflect the size-selectivity of translation and deposition. In the River Calder, $<L>$ is independent of grain size across events with τ_{max} from 0.94 to 2.9 τ_c (Figure 11a). In contrast, the South Fork Eel River and the Allt Dubhaig have an inverse relationship between $<L>$ and tracer size (Figures 11b and 11c). All three rivers have a comparable range of relative grain size (d/d_{50}), and so relative grain size is not responsible for the difference in the relationships. Differences in shear stress are also not responsible; τ^* is higher in the South Fork Eel and the Allt Dubhaig than in the River Calder. As described below, this would predict the opposite pattern of size-selective transport to that observed. In the River Calder, the uniformity of L across grain sizes is consistent with the theoretical and field results that E_b, i.e. re-entrainment of grains in transport, is not size-selective (Figure 3). Although other components of grain transport, e.g. T_b, may be size selective the overriding control on travel distances is the relative ease of transport over bedrock surfaces and the contrast between D_a and D_b.

The South Fork Eel River and Allt Dubhaig results are supported by tracer data from other alluvial rivers where multiple size classes spanning d_{50} have been tracked for multiple events [e.g. *Church and Hassan*, 1992]. Tracer travel distances in the Rio Cordon change from size-dependent to size-independent as a function of increasing discharge [*Lenzi*, 2004]. At low discharges L decreased rapidly with increasing grain size, but at a discharge 15 times threshold ($\tau/\tau_c \approx 4$) L for all but the largest size class ($d/d_{50} = 4.8$) were size independent. Size independent bedload transport (i.e. bedload GSD is equal to the sediment surface GSD) has been recorded in other alluvial rivers when τ/τ_c is greater than 1.5 to 2 [*Parker et al.*, 1982; *Andrews*, 1983; *Wilcock and McArdell,* 1993]; these rivers plot with Oak Creek in Figure 4. However, the hydraulic regime of most alluvial rivers means that typical flows are not substantially above threshold [*Parker* 1978] and therefore the effect of multiple flow events is net size selectivity and divergence in bedload flux, plotting with the Allt Dubhaig in Figure 4 [*Lisle*, 1995]. The integrative nature of tracer data means that it is difficult to identify which component(s) of transport contribute most to the observed size-selectivity. The transition with increasing shear stress, however, suggests a change in the size-selectivity of E_a [*Wilcock*, 1997].

5.4 Distribution of sediment cover and channel morphology

Our three datasets demonstrate how the volume of sediment within a channel affects the dynamics of entrainment, translation and deposition, and hence the reach-scale sediment flux. Both entrainment processes and depositional sorting are affected by surface sediment structure and vertical sorting, and so sediment depth becomes an important factor affecting sediment dynamics and may account for the differences in the size-selectivity of E_a between the rivers.

At low sediment volumes, interactions between bedrock geometry and local hydraulics will control the locations of sediment cover [*Johnson and Whipple*, 2007; *Chatanantavet and Parker*, 2008; *Goode and Wohl*, 2010a, 2010b]. Bedrock geometry stems from the interaction between the river and the resistant bed, via the bed roughness, and is a function of the local geology. Consequently, sediment patches will tend to be irregularly spaced, as in the River Calder (Figure 5). At greater sediment volumes, sediment cover becomes more uniform and bedforms may develop. Regular bedforms could provide a new control on the locations of grain deposition and hence transport lengths [*Pyrce and Ashmore*, 2003a, b]. Across the

837 spectrum of sediment cover, lateral variations in shear stress may cause spatial
838 variations in grain size that in turn produce size-selectivity in entrainment and
839 transport [*Paola and Seal*, 1995].
840
841 As the volume of sediment in a bedrock channel increases, sediment thickness will
842 also increase. Sediment depth in the River Calder is generally less than $2d_{90}$ (Figure
843 5). The majority of sediment is therefore within the active layer and there is no
844 longer-term storage at depth. In addition, surface coarsening, which controls size-
845 selection in entrainment and bedload, cannot develop. Consequently, the volume of
846 sediment stored in a bedrock reach and its spatial distribution together control long-
847 term sorting processes. Surface coarsening is a dynamic response to the protrusion of
848 large grains and the hiding of smaller ones and results, in part, from smaller grains
849 being deposited in deep pores and effectively removed from the active layer [*Allan*
850 *and Frostick* 1999]. Kinematic sorting further enhances the selective removal of
851 smaller grains [*Parker and Sutherland*, 1990; *Frey and Church* 2010]. In beds with a
852 coarse surface layer, D_a and specifically deposition depth, may be size dependent,
853 leading to smaller tracers being mixed more rapidly into the bed than larger ones
854 [*Ferguson and Hoey*, 2002; *Haschenburger,* 2011].
855
856 The development of a coarse surface layer alters the surface GSD and the geometry of
857 grains in the bed, and hence changes the grain-size specific τ_c. Initial entrainment
858 from alluvial patches in the River Calder is weakly size-selective; although
859 entrainment is a function of grain weight, size-selectivity is weak due to the effects of
860 surrounding grains on grain exposure and pivoting angles. Surface coarsening over-
861 represents large grains in the surface, so that at high relative shear stresses the bedload
862 GSD is equal to the sub-surface GSD. However, at lower relative shear stresses,
863 entrainment is still biased towards smaller grains [*Wilcock and McArdell,* 1993;
864 *Powell et al.*, 2001]. Over a range of flows, entrainment from beds with coarse surface
865 layers is somewhat size-dependent leading to size-selective tracer movement distances
866 as observed in the South Fork Eel River and the Allt Dubhaig. Such size-selective
867 entrainment may produce aggradation; if so, unless large floods periodically clear the
868 channel [e.g. *Lague*, 2010], the river will eventually become alluvial.
869
870 The field results show that sediment cover extent can affect channel transport
871 capacity. Bedrock channels with lower sediment cover and otherwise equal
872 characteristics could have a higher transport capacity because of bedrock surfaces
873 facilitating grain transport. The low probability of deposition means that once exposed
874 a bedrock surface will tend to stay exposed. Transport capacity is hence limited by the
875 alluvial patches, and so fractional exposure is a first-order control on transport
876 capacity. Net sediment flux, however, will be limited by supply rather than transport.
877 The role of sediment cover means that supply can affect transport distances; if lower
878 supply reduces sediment cover, then transport velocities will increase. However, the
879 above may only apply if the bedrock is relatively smooth; on a rough bed increased
880 sediment cover could reduce the meso-scale roughness, reducing form drag and
881 increasing sediment transport capacity. Equally, at higher sediment cover, velocities
882 may increase through increased sediment supply because deposition niches in the bed
883 get filled [*Lisle and Church*, 2002].

6 Implications

The idea that sediment processes vary as a function of the amount of sediment in a bedrock channel has implications for understanding and modelling bedrock river evolution. Predicting the distribution of sediment flux and sediment cover throughout a channel network is significant for understanding landscape evolution and has management applications. Rivers with bedrock reaches are widespread and effective management of such rivers, for example in managing the effects of hydropower schemes on instream biota, requires prediction of how sediment flux and cover will vary under given conditions.

A common approach to modelling bedrock rivers is to assume that all sediment can be represented by a single grain size [e.g. *Lague*, 2010] and/or is equally mobile [e.g. *Sklar et al.*, 2006; *Stark et al.*, 2009]. Although these assumptions are broadly consistent with the River Calder data and the sediment continuity analysis, the South Fork Eel River data show that this assumption is invalid when the river contains significant sediment cover. Bedrock river models therefore need to allow for a continuum of sediment processes, as in Figure 1. The location of a reach along this continuum will depend on both the spatial extent and depth of sediment cover. Further research is necessary to identify whether the transition between bedrock and alluvial styles is linear along this continuum. There is also a need to consider the role of pebble abrasion, which has been discounted in this study but which is significant in many bedrock rivers; abrasion can produce downstream fining in a bedrock river where transport is not size-selective [*Attal and Lavé*, 2009]. The rate of downstream fining also depends on the interaction between abrasion and longitudinal variation in the GSD of local sediment supply [*Sklar et al.*, 2006; *Chatanantavet et al.*, 2010].

Over the timescales of relevance to landscape evolution, the rate of sediment supply to a river varies considerably [*Stark et al.* 2009]. Such variations will alter the amount of sediment in the channel and therefore the location of reaches along the alluvial-bedrock continuum [*Sklar and Dietrich*, 2008]. River reaches could thus switch between alluvial and bedrock-style behaviour [*Lague*, 2010]. The possibility for size selective transport in bedrock rivers questions the extent to which such rivers are in long-term equilibrium, given that size-selective transport could mean that larger sediment is accumulating in the river. However, the accumulation rate may be sufficiently slow such that the channel is in a quasi-stable equilibrium, or accumulation may be offset by abrasion. A complete understanding also needs to consider the distributions of discharge, sediment supply and GSD entering these rivers [*Lague*, 2010].

7 Conclusions

Processes of grain entrainment, translation and deposition vary according to position of a bedrock river along the bedrock-alluvial continuum (Figure 1 and Table 1). We predict that, with the exception of rivers with extremely low sediment cover, grains are primarily entrained from alluvial patches. Once in transport, subsequent re-entrainment from a bedrock surface is likely because the necessary shear stresses are an order of magnitude smaller than for entrainment from an alluvial surface (Figure 3). Grains are correspondingly more likely to be deposited on alluvial surfaces. Both grain entrainment and sediment continuity considerations predict that sediment transport in a predominantly bedrock channel should not, in the absence of abrasion, be significantly size-selective.

Gravel tracer data from three rivers across the spectrum of bedrock and alluvial channels have been used to test these theoretical predictions: the River Calder (20 % sediment cover), the South Fork Eel River (80 %) and the alluvial Allt Dubhaig (100 %). Key differences were identified between the three sets of tracer data, namely: 1) in the South Fork Eel River and Allt Dubhaig, distributions of tracer travel distances are adequately described by gamma distributions, whereas the River Calder tracers show multi-modal transport distances; 2) transport distances in the River Calder were size independent across shear stresses up to 2.9 τ/τ_c, whereas both the South Fork Eel River and the Allt Dubhaig demonstrated size selectivity; 3) grains in the River Calder had higher virtual velocities than grains in a directly comparable reach of the Allt Dubhaig; and 4) grains in the River Calder were entrained at a lower value of τ_c* than is typically observed in alluvial rivers.

The empirical findings concur with the theoretical predictions, and are explained by the effect of sediment cover and depth on the components of sediment transport. Despite entrainment primarily occurring from alluvial surfaces in all rivers, entrainment occurs at a lower dimensionless shear stress in the River Calder. This is hypothesised to be because the sparse sediment patches are loosely packed; shallow sediment depths mean that all sediment is frequently mobilised and that surface coarsening is inhibited. The loose packing also means that entrainment is more weakly size selective than in the fully alluvial case.

In the River Calder, sediment is mainly translated across bedrock surfaces. As predicted by the theoretical modelling, grains are not deposited on bedrock surfaces but instead are transported between, and deposited on, sediment patches producing the irregular distribution of transport lengths. The minimal variation in entrainment shear stress with grain size predicted by the theoretical grain model means that there is no significant difference in transport lengths as a function of grain size. The relative ease of transport across bedrock surfaces also results in the higher virtual velocities identified in the River Calder. In contrast, the more complete sediment cover in the South Fork Eel River and Allt Dubhaig means that sediment step lengths are more directly a function of diffusion processes although the scale of bedforms constrains these. The deeper sediment deposits enable surface coarsening to develop, which affects the size-selectivity of grain entrainment and deposition.

The theoretical and field results identify a continuum in sediment processes between alluvial and bedrock rivers. This continuum indicates that models of bedrock rivers can neither assume that all transport is size independent, nor unquestioningly apply formulas developed from alluvial data. Instead, there is a need to consider how the spatial extent and depth of sediment cover affect sediment processes. The data presented in this paper have been used to identify these key controls; these data however only represent three points along the continuum. Further empirical and modelling work is needed to quantify sediment processes along this continuum.

Acknowledgments

Funding was provided by the John Robertson Bequest, University of Glasgow. For the River Calder, thanks to the Clyde Muirshiel Regional Park for access and flow information, to Kenny Roberts for field support and Florenz Hollebrandse for previous data. Allt Dubhaig data was collected in projects funded by NERC led by Rob Ferguson, who provided valuable comments on an earlier draft of this paper. For the South Fork Eel River, thanks to Bill Dietrich, Mary Power, Peter Steele, Martin Trso, Leslie Ferguson, Douglas Allen and many others. Funding was provided by the U.C. Natural Reserve System Mildred E. Mathias Research Grant. Reviews and comments from Jens Turowski, Gary Parker, an anonymous reviewer, the associate editor and the editor improved an earlier version of this paper.

988 **References**

989 Allan, A. F., and L. Frostick (1999), Framework dilation, winnowing, and matrix
990 particle size: The behavior of some sand-gravel mixtures in a laboratory
991 flume, *J. Sediment Res.*, *69*(1), 21-26.

992 Andrews, E. D. (1983), Entrainment of gravel from naturally sorted riverbed material,
993 *Geol. Soc. Am. Bull.*, *94*(10), 1225-1231.

994 Attal, M., and J. Lavé (2009), Pebble abrasion during fluvial transport: Experimental
995 results and implications for the evolution of the sediment load along rivers, *J.*
996 *Geophys. Res.*, *114*, 22 PP., doi:200910.1029/2009JF001328.

997 Bradley, D. N., G. E. Tucker, and D. A. Benson (2010), Fractional dispersion in a
998 sand bed river, *J. Geophys. Res.*, *115*, doi:10.1029/2009JF001268.

999 Buffington, J. M., W. E. Dietrich, and J. W. Kirchner (1992), Friction angle
1000 measurements on a naturally formed gravel streambed - implications for
1001 critical boundary shear-stress, *Water Resour. Res.*, *28*(2), 411-425.

1002 Buffington, J. M., and D. R. Montgomery (1997), A systematic analysis of eight
1003 decades of incipient motion studies, with special reference to gravel-bedded
1004 rivers, *Water Resour. Res.*, *33*(8), PP. 1993-2029,
1005 doi:199710.1029/96WR03190.

1006 Chatanantavet, P., E. Lajeunesse, G. Parker, L. Malverti, and P. Meunier (2010),
1007 Physically based model of downstream fining in bedrock streams with lateral
1008 input, *Water Resour. Res.*, *46*, doi:10.1029/2008WR007208.

1009 Chatanantavet, P., and G. Parker (2008), Experimental study of bedrock channel
1010 alluviation under varied sediment supply and hydraulic conditions, *Water*
1011 *Resour. Res.*, *44*(12), doi:10.1029/2007WR006581.

1012 Church, M., and M. A. Hassan (1992), Size and distance of travel of unconstrained
1013 clasts on a streambed, *Water Resour. Res.*, *28*(1), 299-303.

1014 Cowie, P. A., A. C. Whittaker, M. Attal, G. Roberts, G. E. Tucker, and A. Ganas
1015 (2008), New constraints on sediment-flux-dependent river incision:
1016 Implications for extracting tectonic signals from river profiles, *Geology*, *36*(7),
1017 535-538, doi:10.1130/G24681A.1.

1018 Dancey, C., P. Diplas, A. Papanicolaou, and M. Bala (2002), Probability of individual
1019 grain movement and threshold condition, *J. Hydraul. Eng.-ASCE*, *128*(12),
1020 1069-1075, doi:10.1061/(ASCE)0733-9429(2002)128:12(1069).

1021 DeVries, P. (2002), Bedload layer thickness and disturbance depth in gravel bed
1022 streams, *J. Hydraul. Eng.-ASCE*, *128*(11), 983-991, doi:10.1061/(ASCE)0733-
1023 9429(2002)128:11(983).

1024 Drake, T. G., R. L. Shreve, W. E. Dietrich, P. J. Whiting, and L. B. Leopold (1988),
1025 Bedload transport of fine gravel observed by motion-picture photography, *J.*
1026 *Fluid Mech.*, *192*, 193-217, doi:10.1017/S0022112088001831.

1027 Eagleson, P. S., and R. G. Dean (1961), Wave-Induced Motion of Bottom Sediment
1028 Particles, *Trans. Am. Soc. Civ. Engrs.*, *126*(1), 1162-1189.

1029 Einstein, H. A. (1950), *The bed-load function for sediment transportation in open*
1030 *channel flows*, U.S. Dept. of Agriculture, Washington.

1031 Fenton, J. D., and J. E. Abbott (1977), Initial movement of grains on a stream bed -
1032 effect of relative protrusion, *P. Roy. Soc. Lond. A Mat.*, *352*(1671), 523-537.

1033 Ferguson, R. I., D. J. Bloomer, T. B. Hoey, and A. Werritty (2002), Mobility of river
1034 tracer pebbles over different timescales, *Water Resour. Res.*, *38*(5),
1035 doi:10.1029/2001WR000254.

1036 Ferguson, R. I., and T. B. Hoey (2002), Long-term slowdown of river tracer pebbles:
1037 Generic models and implications for interpreting short-term tracer studies,
1038 *Water Resour. Res.*, *38*(8), doi:10.1029/2001WR000637.

1039 Ferguson, R., T. Hoey, S. Wathen, and A. Werritty (1996), Field evidence for rapid
1040 downstream fining of river gravels through selective transport, *Geology*, *24*(2),
1041 179-182.

1042 Finnegan, N. J., L. S. Sklar, and T. K. Fuller (2007), Interplay of sediment supply,
1043 river incision, and channel morphology revealed by the transient evolution of
1044 an experimental bedrock channel, *J. Geophys. Res.*, *112*(F3),
1045 doi:10.1029/2006JF000569.

1046 Frey, P., and M. Church (2010), Bedload: a granular phenomenon, *Earth. Surf. Proc.*
1047 *Land.*, n/a-n/a, doi:10.1002/esp.2103.

1048 Fuller, T. K., L. A. Perg, J. K. Willenbring, and K. Lepper (2009), Field evidence for
1049 climate-driven changes in sediment supply leading to strath terrace formation,
1050 *Geology*, *37*(5), 467-470, doi:10.1130/G25487A.1.

1051 Gasparini, N., G. Tucker, and R. Bras (2004), Network-scale dynamics of grain-size
1052 sorting: Implications for downstream fining, stream-profile concavity, and
1053 drainage basin morphology, *Earth. Surf. Proc. Land.*, *29*(4), 401-421,
1054 doi:10.1002/esp.1031.

1055 Goode, J. R., and E. Wohl (2010a), Substrate controls on the longitudinal profile of
1056 bedrock channels: Implications for reach-scale roughness, *J. Geophys. Res.*,
1057 *115*(F3), doi:10.1029/2008JF001188.

1058 Goode, J. R., and E. Wohl (2010b), Coarse sediment transport in a bedrock channel
1059 with complex bed topography, *Water Resour. Res.*, *46*(11),
1060 doi:10.1029/2009WR008135.

1061 Grass, A. J. (1970), Initial instability of fine bed sand., *J. Hydraul. Eng.-ASCE*, 619-
1062 632.

1063 Habersack, H. M. (2001), Radio-tracking gravel particles in a large braided river in
1064 New Zealand: a field test of the stochastic theory of bed load transport
1065 proposed by Einstein, *Hydrol. Process.*, *15*(3), 377-391.

1066 Haschenburger, J. K. (2011), Vertical mixing of gravel over a long flood series, *Earth*
1067 *Surf. Process. Landforms*, *36*(8), 1044-1058, doi:10.1002/esp.2130.

1068 Hassan, M. A., M. Church, and A. P. Schick (1991), Distance of movement of coarse
1069 particles in gravel bed streams, *Water Resour. Res.*, *27*(4), 503-511.

1070 Hassan, M. A., A. P. Schick, and J. B. Laronne (1984), The recovery of flood
1071 dispersed coarse sediment particles - a 3-dimensional magnetic tracing
1072 method, *Catena*, 153-162.

1073 Hassan, M. A., M. Church, and P. J. Ashworth (1992), Virtual rate and mean distance
1074 of travel of individual clasts in gravel-bed channels, *Earth. Surf. Proc. Land.*,
1075 *17*(6), 617-627, doi:10.1002/esp.3290170607.

1076 Howard, A. D. (1998), Long profile development of bedrock channels: interaction of
1077 weathering, mass wasting, bed erosion, and sediment transport, in *Rivers over*
1078 *rock: Fluvial processes in bedrock channels*, edited by K. J. Tinkler and E. E.
1079 Wohl, p. 237–260, American Geophysical Union.

1080 Howard, A., and G. Kerby (1983), Channel changes in badlands, *Geol. Soc. Am. Bull.*,
1081 *94*(6), 739-752.

1082 Jansen, J. (2006), Flood magnitude–frequency and lithologic control on bedrock river
1083 incision in post-orogenic terrain, *Geomorphology*, *82*(1-2), 39-57,
1084 doi:10.1016/j.geomorph.2005.08.018.

1085 Johnson, J. P. L., K. X. Whipple, L. S. Sklar, and T. C. Hanks (2009), Transport
1086 slopes, sediment cover, and bedrock channel incision in the Henry Mountains,
1087 Utah, *J. Geophys. Res.*, *114*(F2), doi:10.1029/2007JF000862.

1088 Johnson, J. P., and K. X. Whipple (2007), Feedbacks between erosion and sediment
1089 transport in experimental bedrock channels, *Earth. Surf. Proc. Land.*, *32*(7),
1090 1048-1062, doi:10.1002/esp.1471.

1091 Johnston, C. E., E. D. Andrews, and J. Pitlick (1998), In situ determination of particle
1092 friction angles of fluvial gravels, *Water Resour. Res.*, *34*(8), 2017-2030.

1093 Kirchner, J. W., W. E. Dietrich, F. Iseya, and H. Ikeda (1990), The variability of
1094 critical shear-stress, friction angle, and grain protrusion in water-worked
1095 sediments, *Sedimentology*, *37*(4), 647-672.

1096 Lague, D. (2010), Reduction of long-term bedrock incision efficiency by short-term
1097 alluvial cover intermittency, *J. Geophys. Res.*, *115*,
1098 doi:10.1029/2008JF001210.

1099 Lajeunesse, E., L. Malverti, and F. Charru (2010), Bed load transport in turbulent
1100 flow at the grain scale: Experiments and modeling, *J. Geophys. Res.*, *115*(F4),
1101 doi:10.1029/2009JF001628.

1102 Lamb, M. P., W. E. Dietrich, and J. G. Venditti (2008), Is the critical Shields stress
1103 for incipient sediment motion dependent on channel-bed slope?, *J. Geophys.*
1104 *Res.*, *113*(F2), doi:10.1029/2007JF000831.

1105 Lenzi, M. A. (2004), Displacement and transport of marked pebbles, cobbles and
1106 boulders during floods in a steep mountain stream, *Hydrol. Process.*, *18*(10),
1107 1899-1914, doi:10.1002/hyp.1456.

1108 Lisle, T. E. (1995), Particle size variations between bed load and bed material in
1109 natural gravel bed channels, *Water Resour. Res.*, *31*(4), PP. 1107-1118,
1110 doi:199510.1029/94WR02526.

1111 Lisle, T. E., and M. Church (2002), Sediment transport-storage relations for
1112 degrading, gravel bed channels, *Water Resour. Res.*, *38*(11),
1113 doi:10.1029/2001WR001086.

1114 Montgomery, D. R., T. B. Abbe, J. M. Buffington, N. P. Peterson, K. M. Schmidt, and
1115 J. D. Stock (1996), Distribution of bedrock and alluvial channels in forested
1116 mountain drainage basins, *Nature*, *381*(6583), 587-589,
1117 doi:10.1038/381587a0.

1118 Paola, C., and R. Seal (1995), Grain size patchiness as a cause of selective deposition
1119 and downstream fining, *Water Resour. Res.*, *31*(5), PP. 1395-1407,
1120 doi:199510.1029/94WR02975.

1121 Papanicolaou, A. N., P. Diplas, C. L. Dancey, and M. Balakrishnan (2001), Surface
1122 roughness effects in near-bed turbulence: implications to sediment
1123 entrainment, *J. Engrg. Mech.*, *127*(3), 211-218, doi:10.1061/(ASCE)0733-
1124 9399(2001)127:3(211).

1125 Parker, G. (1991), Selective sorting and abrasion of river gravel .1. Theory, *J.*
1126 *Hydraul. Eng.-ASCE*, *117*(2), 131-149.

1127 Parker, G., P. C. Klingeman, and D. G. McLean (1982), Bedload and size distribution
1128 in paved gravel-bed streams, *J. Hydr. Eng Div.-ASCE*, *108*(4), 544-571.

1129 Parker, G., and A. J. Sutherland (1990), Fluvial armor, *J. Hydraul. Res.*, *28*(5), 529-
1130 544.

1131 Parker, G. (1978), Self-formed straight rivers with equilibrium banks and mobile bed.
1132 Part 2. The gravel river, *J. Fluid Mech.*, *89*(01), 127-146,
1133 doi:10.1017/S0022112078002505.

1134 Powell, D. M., I. Reid, and J. B. Laronne (2001), Evolution of bed load grain size
1135 distribution with increasing flow strength and the effect of flow duration on
1136 the caliber of bed load sediment yield in ephemeral gravel bed rivers, *Water*
1137 *Resour. Res.*, *37*(5), PP. 1463-1474, doi:200110.1029/2000WR900342.

1138 Pyrce, R. S., and P. E. Ashmore (2003a), Particle path length distributions in
1139 meandering gravel-bed streams: Results from physical models, *Earth. Surf.*
1140 *Proc. Land.*, *28*(9), 951-966, doi:10.1002/esp.498.

1141 Pyrce, R. S., and P. E. Ashmore (2003b), The relation between particle path length
1142 distributions and channel morphology in gravel-bed streams: a synthesis,
1143 *Geomorphology*, *56*(1-2), 167-187, doi:10.1016/S0169-555X(03)00077-1.

1144 Recking, A. (2009), Theoretical development on the effects of changing flow
1145 hydraulics on incipient bed load motion, *Water Resour. Res.*, *45*(4),
1146 doi:10.1029/2008WR006826.

1147 Schmeeckle, M. W., and J. M. Nelson (2003), Direct numerical simulation of bedload
1148 transport using a local, dynamic boundary condition, *Sedimentology*, *50*(2),
1149 279-301, doi:10.1046/j.1365-3091.2003.00555.x.

1150 Schmidt, K. H., and P. Ergenzinger (1992), Bedload entrainment, travel lengths, step
1151 lengths, rest periods - studied with passive (iron, magnetic) and active (radio)
1152 tracer techniques, *Earth. Surf. Proc. Land.*, *17*(2), 147-165.

1153 Seidl, M. A., and W. E. Dietrich (1992), The problem of channel erosion into
1154 bedrock, in *Functional geomorphology: landform analysis and models,*
1155 *Catena Supplement 23*, edited by K. H. Schmidt, edited by , de Ploey, pp. 101-
1156 124.

1157 Shvidchenko, A. B., G. Pender, and T. B. Hoey (2001), Critical shear stress for
1158 incipient motion of sand/gravel streambeds, *Water Resour. Res.*, *37*(8), 2273-
1159 2283, doi:200110.1029/2000WR000036.

1160 Siddiqui, A., and A. Robert (2010), Thresholds of erosion and sediment movement in
1161 bedrock channels, *Geomorphology*, *118*(3-4), 301-313,
1162 doi:10.1016/j.geomorph.2010.01.011.

1163 Sklar, L. S., and W. E. Dietrich (2001), Sediment and rock strength controls on river
1164 incision into bedrock, *Geology*, *29*(12), 1087-1090.

1165 Sklar, L. S., and W. E. Dietrich (2004), A mechanistic model for river incision into
1166 bedrock by saltating bed load, *Water Resour. Res.*, *40*, W06301,
1167 doi:10.1029/2003WR002496.

1168 Sklar, L. S., and W. E. Dietrich (2006), The role of sediment in controlling steady-
1169 state bedrock channel slope: Implications of the saltation–abrasion incision
1170 model, *Geomorphology*, *82*(1-2), 58-83, doi:10.1016/j.geomorph.2005.08.019.

1171 Sklar, L. S., and W. E. Dietrich (2008), Implications of the saltation–abrasion bedrock
1172 incision model for steady-state river longitudinal profile relief and concavity,
1173 *Earth Surf. Process. Landforms*, *33*(7), 1129-1151, doi:10.1002/esp.1689.

1174 Sklar, L. S., W. E. Dietrich, E. Foufoula-Georgiou, B. Lashermes, and D. Bellugi
1175 (2006), Do gravel bed river size distributions record channel network
1176 structure?, *Water Resour. Res.*, *42*(6), doi:10.1029/2006WR005035.

1177 Stark, C. P., E. Foufoula-Georgiou, and V. Ganti (2009), A nonlocal theory of
1178 sediment buffering and bedrock channel evolution, *J. Geophys. Res.*, *114*(F1),
1179 doi:10.1029/2008JF000981.

1180 Tinkler, K. J., and E. E. Wohl (1998), *Rivers over rock: Fluvial processes in bedrock*
1181 *channels*, American Geophysical Union.

1182 Turowski, J. M. (2009), Stochastic modeling of the cover effect and bedrock erosion,

Water Resour. Res., *45*, doi:10.1029/2008WR007262.

Turowski, J. M., D. Lague, and N. Hovius (2007), Cover effect in bedrock abrasion: A new derivation and its implications for the modeling of bedrock channel morphology, *J. Geophys. Res.*, *112*(F4), doi:10.1029/2006JF000697.

Turowski, J. M., N. Hovius, A. Wilson, and M.-J. Horng (2008), Hydraulic geometry, river sediment and the definition of bedrock channels, *Geomorphology*, *99*(1-4), 26-38, doi:10.1016/j.geomorph.2007.10.001.

Whipple, K. (2004), Bedrock rivers and the geomorphology of active orogens, *Annu. Rev. Earth Planet. Sci.*, *32*, 151-185, doi:10.1146/annurev.earth.32.101802.120356.

Wiberg, P. L., and J. D. Smith (1987), Calculations of the critical shear stress for motion of uniform and heterogeneous sediments, *Water Resour. Res.*, *23*(8), 1471–1480, doi:10.1029/WR023i008p01471.

Wilcock, P. R., and B. W. McArdell (1993), Surface-based fractional transport rates - mobilization thresholds and partial transport of a sand-gravel sediment, *Water Resour. Res.*, *29*(4), 1297-1312.

Wilcock, P. R. (1997), Entrainment, displacement and transport of tracer gravels, *Earth. Surf. Proc. Land.*, *22*(12), 1125-1138.

Wohl, E., and H. Ikeda (1997), Experimental simulation of channel incision into a cohesive substrate at varying gradients, *Geology*, *25*(4), 295 -298.

Wong, M., G. Parker, P. DeVries, T. M. Brown, and S. J. Burges (2007), Experiments on dispersion of tracer stones under lower-regime plane-bed equilibrium bed load transport, *Water Resour. Res.*, *43*(3), doi:10.1029/2006WR005172.

Figure captions

Figure 1: The continuum of channel types resulting from different degrees of sediment cover. a) Cartoons illustrating different extents of alluvial cover along the continuum between fully bedrock and alluvial channels. b) It is hypothesised that differences in size-selectivity are the result of the processes of grain entrainment (E), translation (T) and deposition (D) occurring from either bedrock or alluvial areas (e.g. E_b or E_a). The sequences show the combination of these processes that are expected to occur in each of the different channel types, as illustrated by the arrows in (a). The other possible combinations $E_a - T_a - D_b$, $E_b - T_a - D_a$ and $E_b - T_a - D_b$ are considered to be unlikely to occur in any setting. c) Study sites that represent each channel form.

Figure 2: Grain geometry in: a) alluvial; and, b) bedrock cases. Bedrock is approximated by an alluvial surface with low surface roughness. Overlying grains (with diameter d) are black, underlying grains (with diameter K) are grey. c) For each pair of d and K on an alluvial surface, Φ is calculated as $\Phi = 51.6\left(d/K\right)^{-0.30}$; coefficient values were calculated from field measurements by *Johnston et al.* [1998] in Sagehen Creek (steep mountain stream, d_{50} = 58 mm), which is the most similar of their study rivers to the River Calder. On a bedrock surface,

1224 $\Phi = \tan^{-1}\left(\gamma \Big/ \sqrt{(d/K)^2 + 2(d/K) - (1/3)}\right)$, which represents pivoting from a pocket
1225 formed by three grains [*Eagleson and Dean*, 1961]. The former alluvial relationship
1226 for Φ incorporates the effect of surrounding grains on Φ, whereas the latter bedrock
1227 relationship better represents grains pivoting on a solid surface. Grain exposure e is
1228 measured from local upstream maximum elevation and calculated as
1229 $e = 0.5[d - K + (d + K)\cos\Phi]$. Grain protrusion p is measured from local mean bed
1230 surface elevation as $p = e + (\pi/12)K$. When calculating p and e, all underlying grains
1231 are assumed to be the same size.
1232
1233 Figure 3: Distributions of: a) τ_c and b) τ_c* for 1000 grains in each of an alluvial and
1234 bedrock setting. Markers are shaded according to K, the size of the underlying grains.
1235 Values for $K = K_{50}$ are shown in black. Note that in (a) grain size is plotted relative to
1236 the median size of the overlying grains (d_{50}) whereas in (b) grain size is plotted
1237 relative to the median size of the underlying grains (K_{50}). The line in (b) shows equal
1238 mobility, i.e. τ_c* is proportional to $1/d$; this line was fitted to theoretical and field data
1239 by *Johnston et al.* [1998]. Comparison between the gradients of the line and the model
1240 results are instructive; the difference in absolute values of τ_c* is less instructive
1241 because of the dependency of τ_c* on model components, e.g. the pivoting angle
1242 relationship.
1243
1244 Figure 4: The dimensional space between proportional sediment cover and degree of
1245 size selectivity of sediment transport distances. Labelled points in this space are Oak
1246 Creek, an alluvial river with no size-selectivity [*Parker et al.*, 1982] and the Allt
1247 Dubhaig, an alluvial river in which size-selectivity varies as a function of excess shear
1248 stress [*Ferguson et al.*, 2002]. The difference in size selectivity between these two is
1249 because Oak Creek has no divergence in sediment transport (∇q_{bT}) so is in steady
1250 state, whereas the Allt Dubhaig has divergence and is hence aggrading. It is
1251 hypothesised that bedrock rivers with low sediment cover cannot be size-selective,
1252 and thus no rivers should plot within the shaded area. However, little data have
1253 previously been collected from such rivers; the bounds of this area are therefore
1254 indicative with darker shading indicating a lower probability of rivers falling within
1255 this area.
1256
1257 Figure 5: The spatial distribution of tracers within the River Calder after four different
1258 sized events. Sediment cover was mapped on a single day. Inset figure shows
1259 distributions of sediment depths at two marked locations. Measurements were taken at
1260 ~ 2 m spacing and d_{90} = 78 mm. Inset picture shows the upper part of the study reach.
1261 Picture taken from place indicated by *, looking downstream.
1262
1263 Figure 6: Time series of mean shear stress (τ), tracer installation and searches in the
1264 River Calder during the experimental period. Day 1 is 16th February 2009. Searches
1265 are numbered. Recovery rates are calculated as a percentage of the number of tracers
1266 in the river; this varies over time as a result of both tracer removal and emplacement.
1267 The recovery rate of search 1 is low because only a partial survey of visible tracers
1268 was undertaken. Histograms show the proportion of installed and found tracers in 5
1269 half psi size classes from 22 to 128 mm. The horizontal line shows τ_c, the threshold
1270 shear stress for sediment transport.
1271

Figure 7: Hydrograph for the South Fork Eel River during the experimental period. Discharge has been calculated from data from Elder Creek, a tributary to the South Fork Eel River within the study reach because the South Fork Eel River was ungauged during the study. Correlation of daily flows from Elder Creek and South Fork Eel River during overlapping gauge records gave $p < 0.0001$. Number of tracers installed and found, and the percentage of found tracers that moved < 1m, are also given. Of the installed tracers, 148/86/62/34 tracers were found 0/1/2/3 times respectively.

Figure 8: a) The probability of tracer initial entrainment as a function of maximum event shear stress (τ_{max}) and tracer starting position on bedrock or on sediment. b) The probability of entrained tracers being deposited on an alluvial surface as a function of maximum event shear stress (τ_{max}). Error bars show 95% confidence intervals for proportions. In both a) and b) the lines show a logistic regression to all relevant tracer data.

Figure 9: Distributions of tracer travel distances (L) from (a-b) the River Calder, (c-e) South Fork Eel River and (f-g) reach T3 of the Allt Dubhaig (grey bars). Data are only shown for tracers that moved. The distribution in (b) for day 155-220 in the River Calder is only for tracers that were in the upstream section of the reach on day 155. All data cover a comparable range of travel distances, with the exception of (a), the River Calder day 1-155. A gamma distribution has been fitted to each dataset (black line); bold values in the left hand table and solid lines indicate no significant difference between the gamma distribution and the field data. The number of tracers in each distribution is shown in the right hand table.

Figure 10: Travel distance of each tracer (grey) and mean travel distances for all tracers in each size class (black) against maximum event shear stress. A power function ($< L >= 3.86 \times 10^{-10} \tau_{\max}^{6.03}$, $R^2 = 0.93$) and a quadratic function ($\log(\tau_{\max}) = 1.56 + 0.10 \log(< L >) + 0.03(\log(< L >)^2)$, $R^2 = 0.97$) are fitted to mean travel distances; dashed and solid black lines respectively. τ_c is determined to be 31 Pa, which is identified by the vertical dashed line.

Figure 11: Relationships between size class, travel distance and shear stress for the River Calder, South Fork Eel River and Allt Dubhaig. For the River Calder, data are plotted according to maximum shear stress. For the South Fork Eel River, data are plotted by year; shear stresses were higher in the first than in the latter two years. For the Allt Dubhaig, data are plotted by reach and are measured over two years. To aid comparison between the rivers, d is plotted as a multiple of reach d_{50}. For all three plots, each symbol represents ≥ 10 tracers. Symbols are offset within each size class to aid clarity. For the River Calder, 0.2 m (dotted line) is the minimum resolvable travel distance. Error bars are the 95% confidence interval for the mean; error bars with values < 0 are not shown.

Figure 12: Relationships between a) virtual velocity and grain size for all Calder tracers emplaced on Day 1, b) total velocity and grain size all South Fork Eel River tracers and c) virtual velocity and grain size for all tracers in reach T3 of the Allt Dubhaig measured over two years. Virtual velocity and total velocity are respectively

calculated using time when flow is above threshold and total experimental time. Mobile tracers are shown by grey closed circles. Grey open circles show the size of immobile tracers. Mean and 95% error bar for the mean for each size class are shown by the horizontal bars and vertical lines; River Calder and Allt Dubhaig data are grouped in half-phi size classes whereas South Fork River Eel data are grouped into four quantile size classes, with size classes being separated by dashed lines. Thick black lines show regressions fitted to the data, which are given by equations (5), (6) and (7) for (a), (b) and (c) respectively.

Tables

Table 1. Properties of the three study rivers

	River Calder	South Fork Eel River	Allt Dubhaig[a]
Sediment cover (%)	20	80	100
Drainage area (km^2)	19	112	13
Channel slope (m/m)	0.009	0.005	0.013
Width (m)	8-13	18	10
Grain size d_{50} (mm)	50	60	61
Reach length (m)	800	3000	450
Discharge, Q_{ma} (m^3s^{-1})[b]	[c]	5	6
Discharge, $Q_{1.5}$ (m^3s^{-1})[d]	10[e]	120	5-7
Depth, $H_{1.5}$ (m)	0.9	2.0	1.2
Shear stress, $\tau_{1.5}$ (Pa)	44	100	73
Shields stress, $\tau^*_{1.5}$	0.054	0.103	0.074

[a]Data are given for Allt Dubhaig reach T3 [*Ferguson et al.*, 2002]
[b]Mean annual discharge
[c]Insufficient flow data to quantify
[d]Discharge with return interval of 1.5 years
[e]Bankfull discharge, estimated assuming Manning's n = 0.05

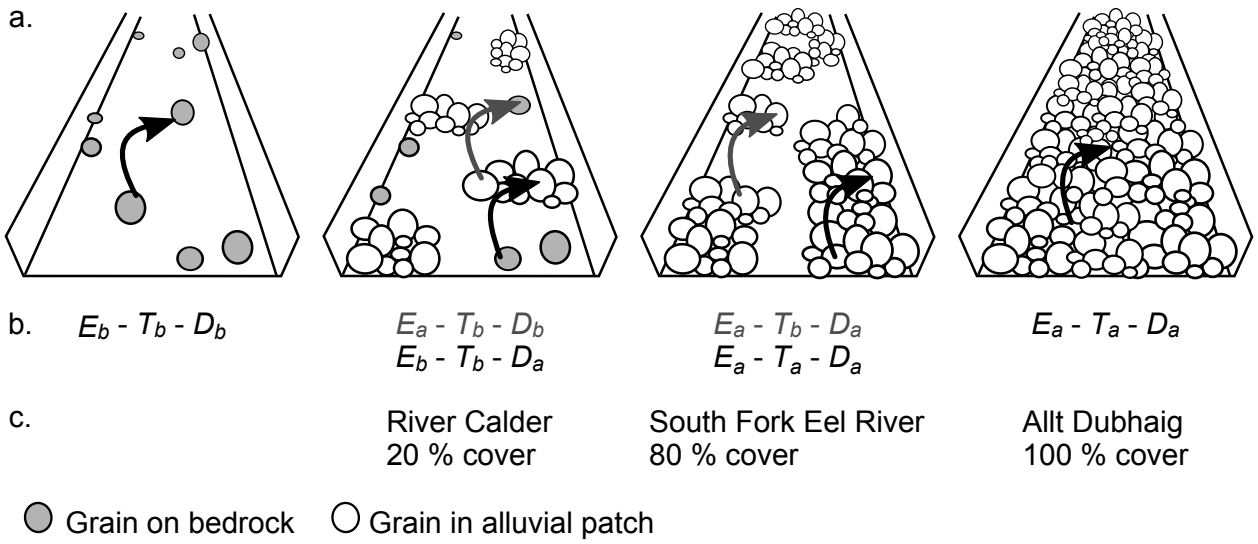

Figure 1: The continuum of channel types resulting from different degrees of sediment cover. a) Cartoons illustrating different extents of alluvial cover along the continuum between fully bedrock and alluvial channels. b) It is hypothesised that differences in size-selectivity are the result of the processes of grain entrainment (E), translation (T) and deposition (D) occurring from either bedrock or alluvial areas (e.g. E_b or E_a). The sequences show the combination of these processes that are expected to occur in each of the different channel types, as illustrated by the arrows in (a). The other possible combinations $E_a – T_a – D_b$, $E_b – T_a – D_a$ and $E_b – T_a – D_b$ are considered to be unlikely to occur in any setting. c) Study sites that represent each channel form.

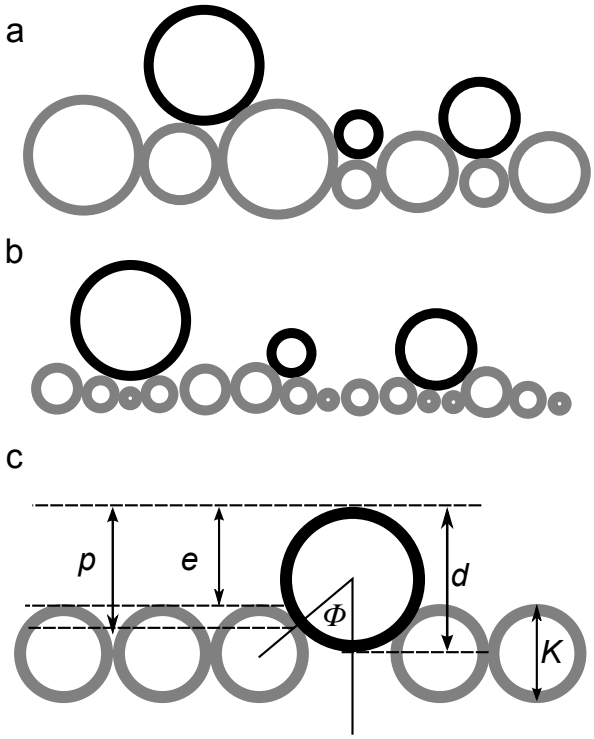

Figure 2: Grain geometry in: a) alluvial; and, b) bedrock cases. Bedrock is approximated by an alluvial surface with low surface roughness. Overlying grains (with diameter d) are black, underlying grains (with diameter K) are grey. c) For each pair of d and K on an alluvial surface, Φ is calculated as $\Phi = 51.6(d/K)^{-0.30}$; coefficient values were calculated from field measurements by *Johnston et al.* [1998] in Sagehen Creek (steep mountain stream, d_{50} = 58 mm), which is the most similar of their study rivers to the River Calder. On a bedrock surface, $\Phi=\text{atan}(\gamma/\sqrt{(d/K)^2+2(d/K)-(1/3)})$, which represents pivoting from a pocket formed by three grains [*Eagleson and Dean*, 1961]. The former alluvial relationship for Φ incorporates the effect of surrounding grains on Φ, whereas the latter bedrock relationship better represents grains pivoting on a solid surface. Grain exposure e is measured from local upstream maximum elevation and calculated as $e = 0.5[d - K + (d + K) \cos \Phi]$. Grain protrusion p is measured from local mean bed surface elevation as $p = e + (\pi/12) K$. When calculating p and e, all underlying grains are assumed to be the same size.

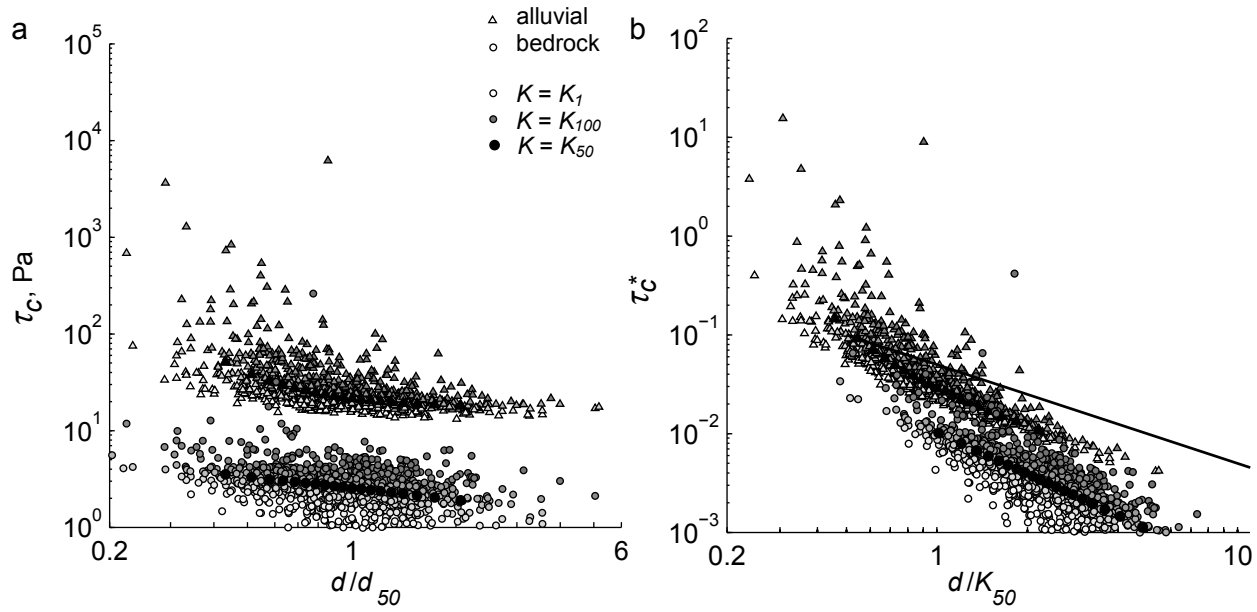

Figure 3: Distributions of: a) τ_c and b) τ_c^* for 1000 grains in each of an alluvial and bedrock setting. Markers are shaded according to K, the size of the underlying grains. Values for $K = K_{50}$ are shown in black. Note that in (a) grain size is plotted relative to the median size of the overlying grains (d_{50}) whereas in (b) grain size is plotted relative to the median size of the underlying grains (K_{50}). The line in (b) shows equal mobility, i.e. τ_c^* is proportional to $1/d$; this line was fitted to theoretical and field data by *Johnston et al.* [1998]. Comparison between the gradients of the line and the model results are instructive; the difference in absolute values of τ_c^* is less instructive because of the dependency of τ_c^* on model components, e.g. the pivoting angle relationship.

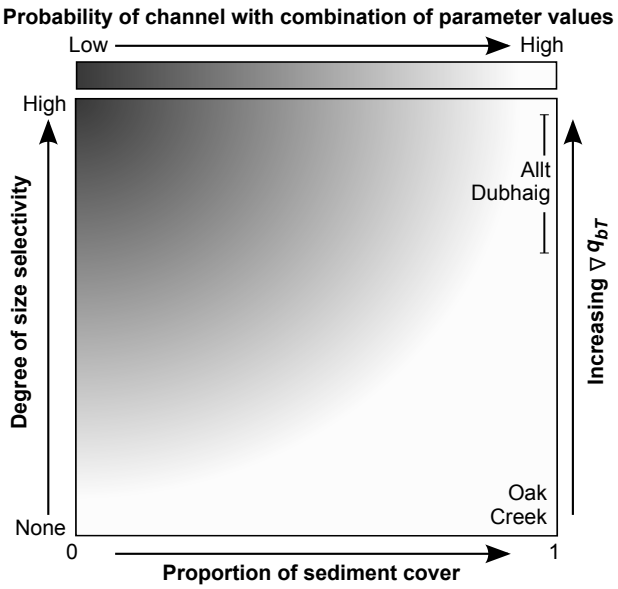

Figure 4: The dimensional space between proportional sediment cover and degree of size selectivity of sediment transport distances. Labelled points in this space are Oak Creek, an alluvial river with no size-selectivity [*Parker et al.*, 1982] and the Allt Dubhaig, an alluvial river in which size-selectivity varies as a function of excess shear stress [*Ferguson et al.*, 2002]. The difference in size selectivity between these two is because Oak Creek has no divergence in sediment transport (∇q_{bT}) so is in steady state, whereas the Allt Dubhaig has divergence and is hence aggrading. It is hypothesised that bedrock rivers with low sediment cover cannot be size-selective, and thus no rivers should plot within the shaded area. However, little data has previously been collected from such rivers; the bounds of this area are therefore indicative with darker shading indicating a lower probability of rivers falling within this area.

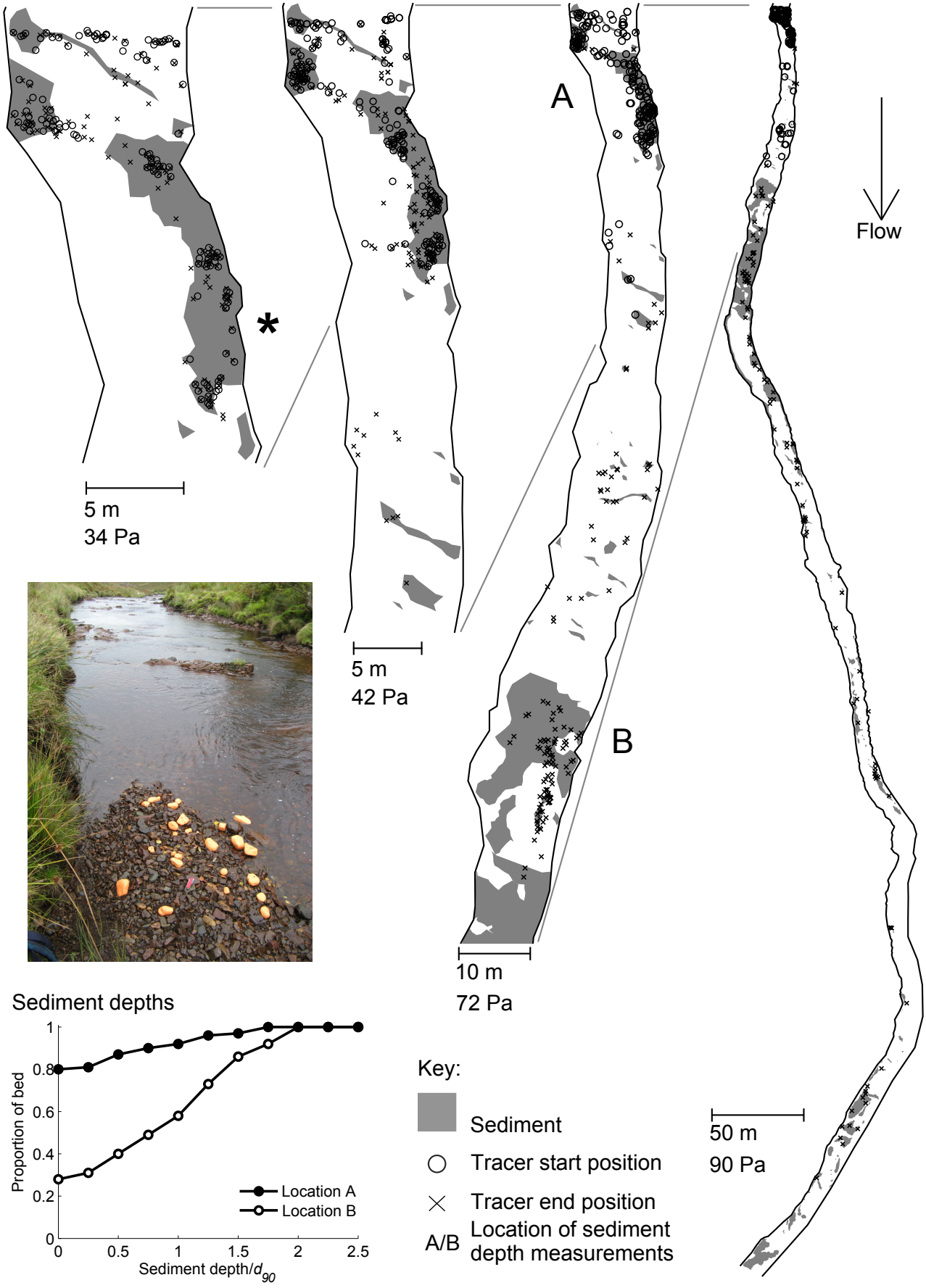

Figure 5: The spatial distribution of tracers within the River Calder after four different sized events. Sediment cover was mapped on a single day. Inset figure shows distributions of sediment depths at two marked locations. Measurements were taken at ~ 2 m spacing and d_{90} = 78 mm. Inset picture shows the upper part of the study reach. Picture taken from place indicated by *, looking downstream.

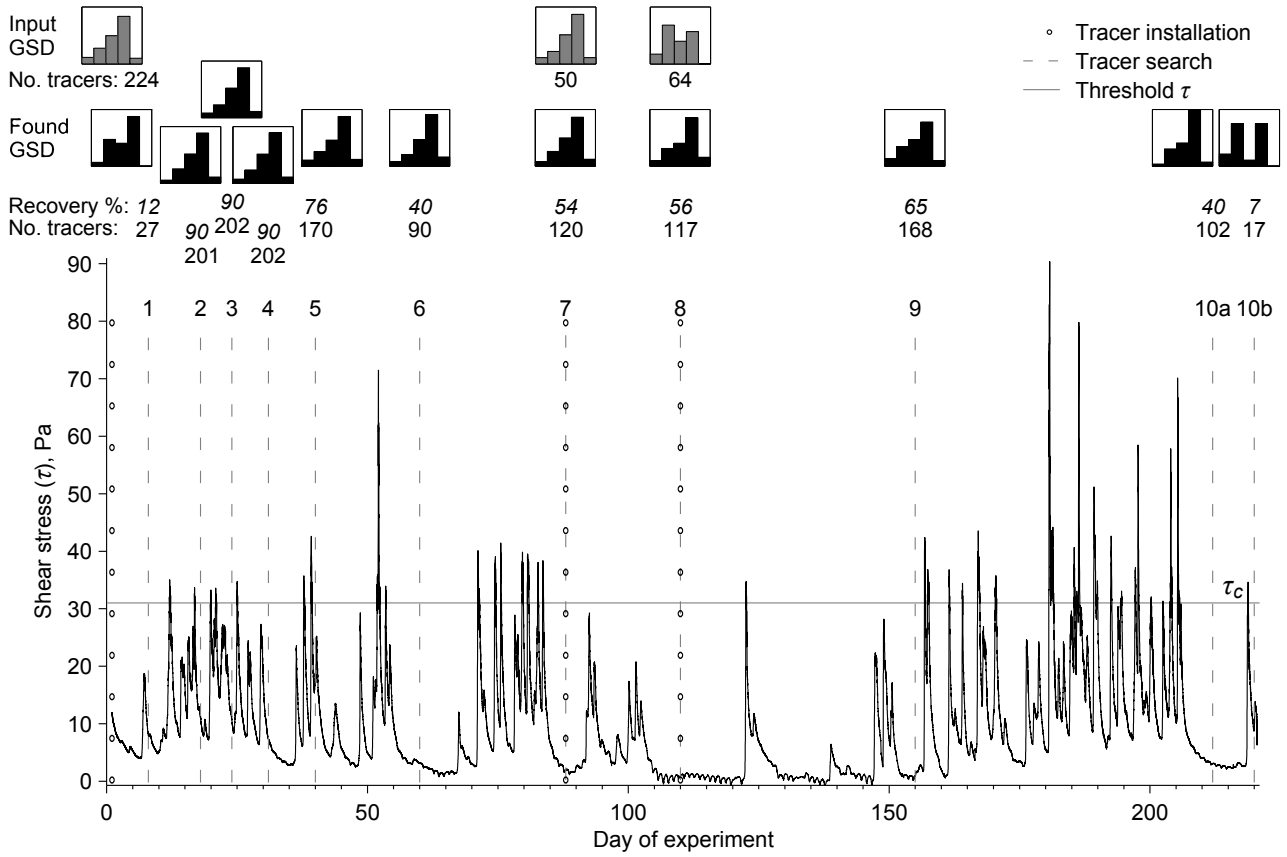

Figure 6: Time series of mean shear stress (τ), tracer installation and searches in the River Calder during the experimental period. Day 1 is 16th February 2009. Searches are numbered. Recovery rates are calculated as a percentage of the number of tracers in the river; this varies over time as a result of both tracer removal and emplacement. The recovery rate of search 1 is low because only a partial survey of visible tracers was undertaken. Histograms show the proportion of installed and found tracers in 5 half psi size classes from 22 to 128 mm. The horizontal line shows τ_c, the threshold shear stress for sediment transport.

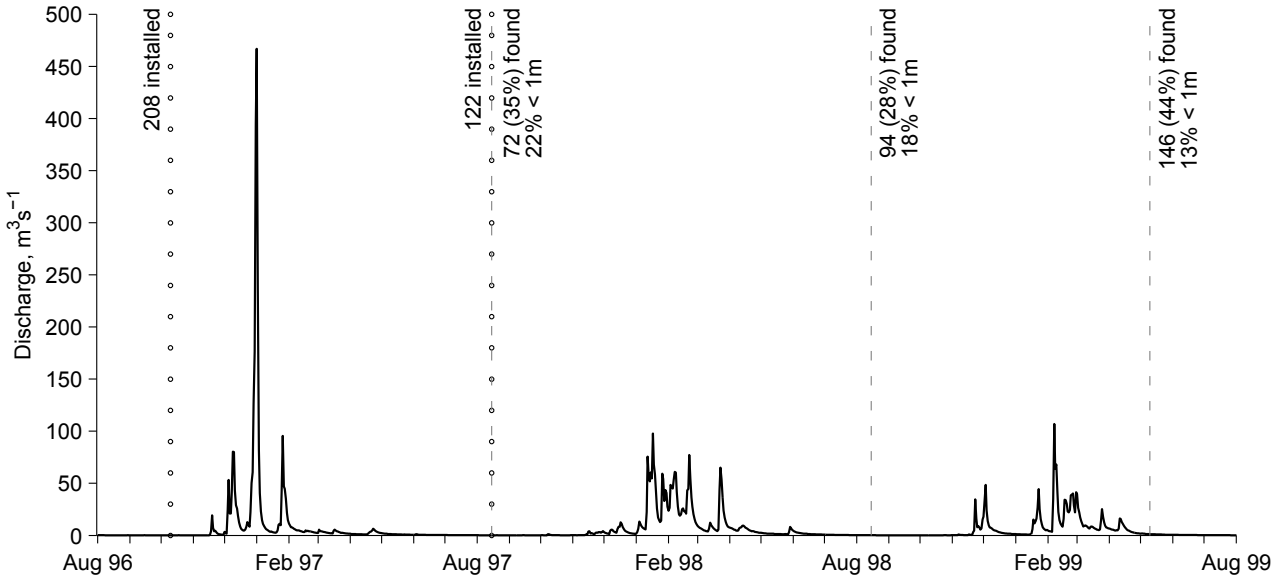

Figure 7: Hydrograph for the South Fork Eel River during the experimental period. Discharge has been calculated from data from Elder Creek, a tributary to the South Fork Eel River within the study reach because the South Fork Eel River was ungauged during the study. Correlation of daily flows from Elder Creek and South Fork Eel River during overlapping gauge records gave $p < 0.0001$. Number of tracers installed and found, and the percentage of found tracers that moved < 1m, are also given. Of the installed tracers, 148/86/62/34 tracers were found 0/1/2/3 times respectively.

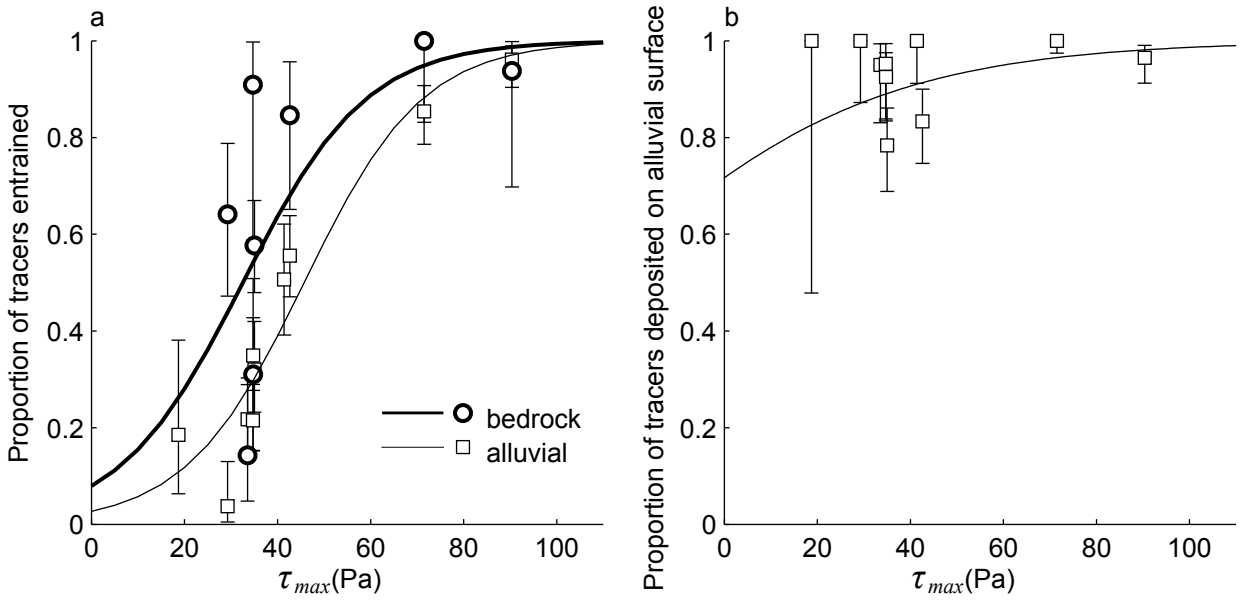

Figure 8: a) The probability of tracer initial entrainment as a function of maximum event shear stress (τ_{max}) and tracer starting position on bedrock or on sediment. b) The probability of entrained tracers being deposited on an alluvial surface as a function of maximum event shear stress (τ_{max}). Error bars show 95% confidence intervals for proportions. In both a) and b) the lines show a logistic regression to all relevant tracer data.

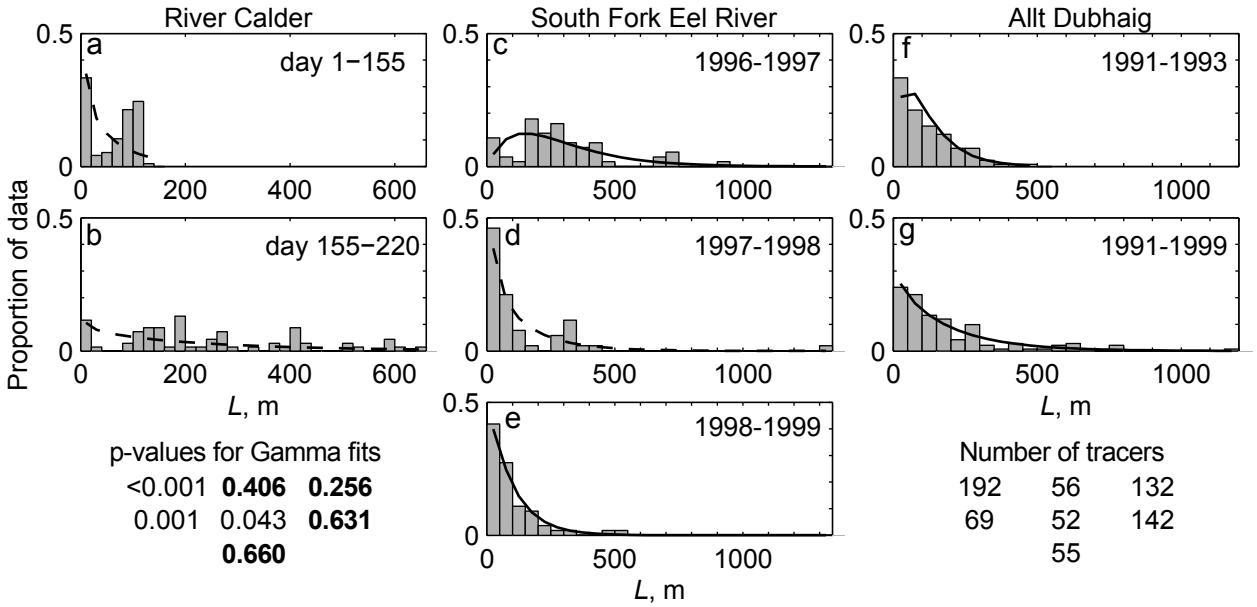

Figure 9: Distributions of tracer travel distances (L) from (a-b) the River Calder, (c-e) South Fork Eel River and (f-g) reach T3 of the Allt Dubhaig (grey bars). Data are only shown for tracers that moved. The distribution in (b) for day 155-220 in the River Calder is only for tracers that were in the upstream section of the reach on day 155. All data cover a comparable range of travel distances, with the exception of (a), the River Calder day 1-155. A gamma distribution has been fitted to each dataset (black line); bold values in the left hand table and solid lines indicate no significant difference between the gamma distribution and the field data. The number of tracers in each distribution is shown in the right hand table.

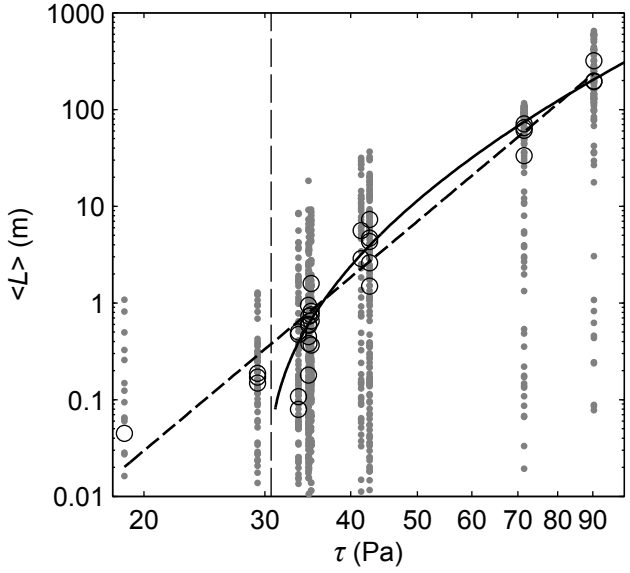

Figure 10: Travel distance of each tracer (grey) and mean travel distances for all tracers in each size class (black) against maximum event shear stress. A power function ($<L>=3.86x10^{-10}\tau_{max}^{6.03}$, $R^2 = 0.93$) and a quadratic function ($\log(\tau_{max}) = 1.56+0.10\log(<L>)+0.03(\log(<L>)2)$, $R^2 = 0.97$) are fitted to mean travel distances; dashed and solid black lines respectively. τ_c is determined to be 31 Pa, which is identified by the vertical dashed line.

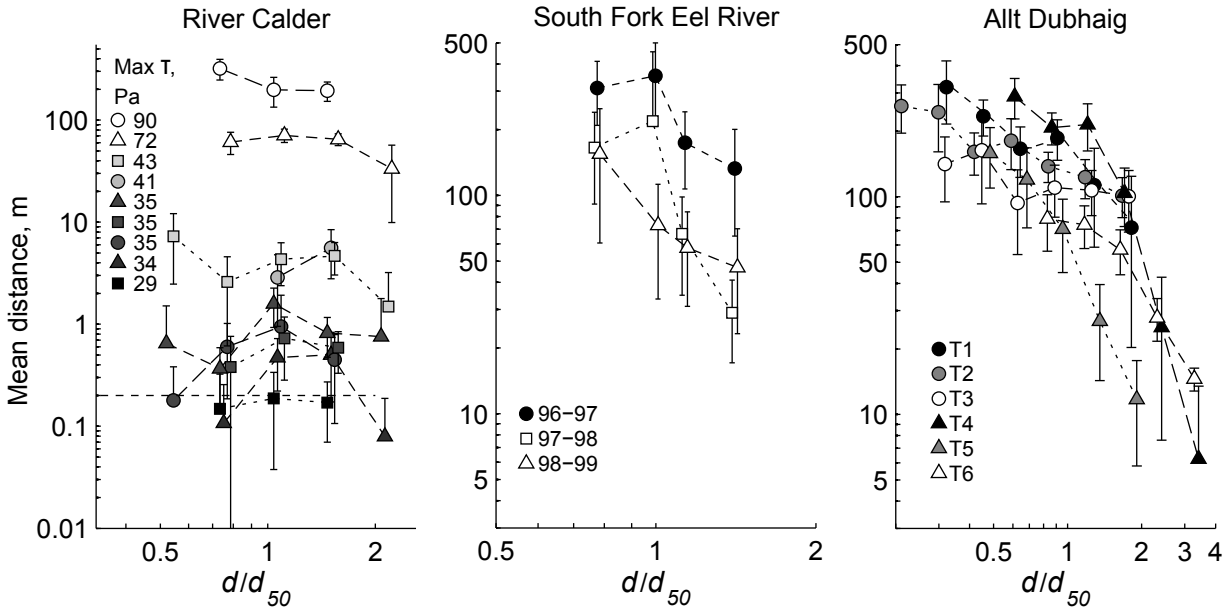

Figure 11: Relationships between size class, travel distance and shear stress for the River Calder, South Fork Eel River and Allt Dubhaig. For the River Calder, data are plotted according to maximum shear stress. For the South Fork Eel River, data are plotted by year; shear stresses were higher in the first than in the latter two years. For the Allt Dubhaig, data are plotted by reach and are measured over two years. To aid comparison between the rivers, d is plotted as a multiple of reach d_{50}. For all three plots, each symbol represents ≥ 10 tracers. Symbols are offset within each size class to aid clarity. For the River Calder, 0.2 m (dotted line) is the minimum resolvable travel distance. Error bars are the 95% confidence interval for the mean; error bars with values < 0 are not shown.

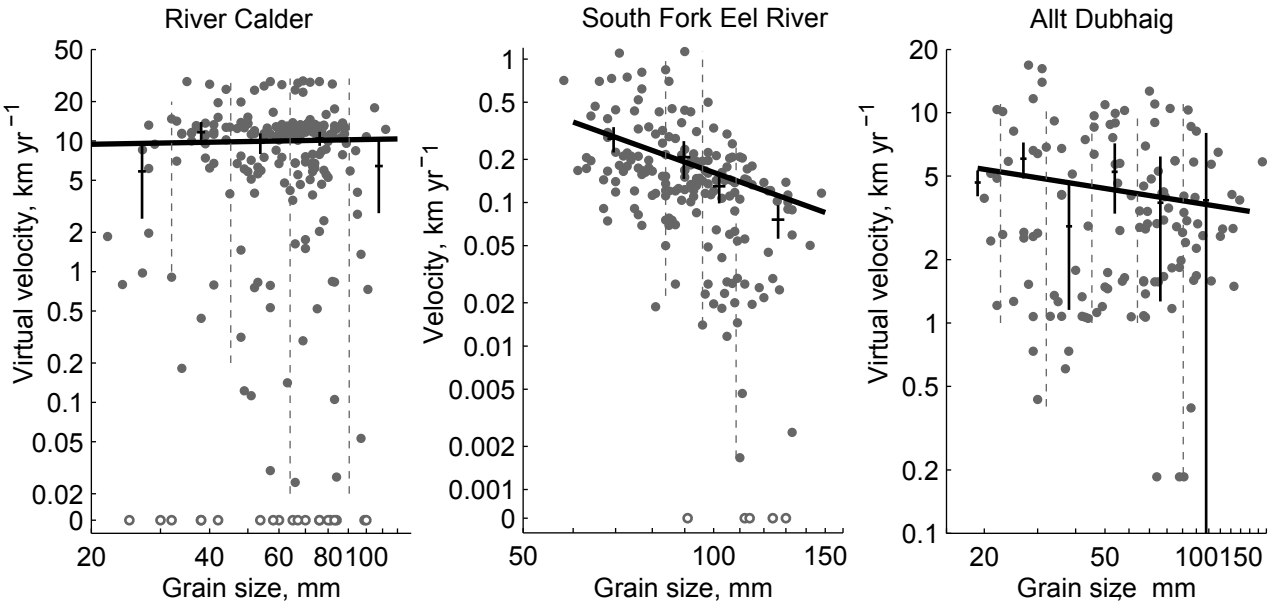

Figure 12: Relationship between virtual velocity and grain size for a) all Calder tracers emplaced on Day 1, b) all South Fork Eel River tracers and c) all tracers in reach T3 of the Allt Dubhaig measured over two years. Mobile tracers are shown by grey closed circles. Grey open circles show the size of immobile tracers. Mean and 95% error bar for the mean for each size class are shown by the horizontal bars and vertical lines; River Calder and Allt Dubhaig data are grouped in half-phi size classes whereas South Fork River Eel data are grouped into four quantile size classes, with size classes being separated by dashed lines. Thick black lines show regressions fitted to the data, which are given by equations (19), (20) and (21) for (a), (b) and (c) respectively.